Supplementary Files

Supplementary Methods

Mutation analyses

Genomic DNA was isolated directly from blood samples by standard methods. Amplification of seven genomic fragments comprising one non-coding exon and all six coding exons of *DNAAF6* was performed as previously described [1]. PCR-products were verified by agarose gel electrophoresis, purified by PCR product pre-sequencing kit (USB, Ohio, USA) and sequenced bi-directionally using BigDye Terminator v3.1 Cycle Sequencing Kit (Applied Biosystems, California, USA). Samples were separated and analysed on an Applied Biosystems 3730xl DNA Analyzer. Sequence data were evaluated using the CodonCode software (CodonCode Corporation, Dedham, USA). The DNA variants identified in *DNAAF6* were classified based on the ACMG/AMP guidelines [2].

Panel Diagnostic

Next Generation Sequencing (NGS) was performed using a diagnostic PCD-gene panel for 51 genes previously associated with PCD and/or laterality defects (Supplementary Table S1) (Agilent Technologies, custom made panel). DNA samples were enriched with SureSelect™ Target Enrichment Kit (Agilent Technologies, Santa Clara, USA). Libraries were sequenced on a MiSeq or a NextSeq 500 platform (Illumina, San Diego, USA) using 2× 150 bp paired-end sequencing. A triple bioinformatics pipeline was set up to secure detection of SNVs and Indels. The first pipeline included the CASAVA suite v1.8.2 from Illumina for demultiplexing, generation of fastq files, mapping of the reads and variant calling. In the second pipeline, reads mapping was performed using Burrow-Wheeler Aligner, recalibration and variant calling were performed using Picard and GATK software; data were imported into a homemade bioinformatics pipeline which mainly based on wANNOVAR backbone [3]. The third pipeline represents the GensearchNGS software tool (PhenoSystems SA). Variants detected by these pipelines were then annotated by Alamut Batch (Interactive BioSoftware, Rouen, France). For each sequencing run, quality reports integrating the number of clusters/mm2, percentage of bases with a Qscore >30, FastQC reports, percentage of mapped reads, on- and off-targets percentages, percentage of covered bases and mean sequencing depth were generated. Detected variants were confirmed on the original blood sample by PCR-amplification of genomic fragments and Sanger sequencing. Our captured design and NGS workflow ensured coverage of more than 99% of targeted bases and a read depth of 50× at all positions. Only at few positions read depth was smaller and those positions were controlled by Sanger sequencing.

Whole Exome Sequencing (WES)

Genomic DNA was isolated directly from blood samples following standard methods. Mutational analysis was performed via exome sequencing (ES) analysis. For ES, extracted genomic DNA was enriched using Agilent Sureselect Clinical Research Exome (CRE) Capture. Samples were run on HiSeq (101 bp paired end, Illumina). On average, 50 million reads per exome and a mapped fraction of >98% were obtained. Average coverage was approximately 50 fold. The data were demultiplexed using the Illumina Software CASAV. Reads were mapped to the human reference genome (GRCh38 and GRCh37) using Burrows-Wheeler Aligner (bio-bwa.sourceforge.net). Variant detection was performed using Genome Analysis Toolkit (www.broadinstitute.org/gatk). Variant Calling Format file was then loaded into Cartagenia in which the filtering of the variants takes place. Variants present in the single nucleotide polymorphism database, the 1000 Genomes Project Database, and the Genome Aggregation Database with a minor-allele frequency of >0.01% were excluded.

Whole Genome Sequencing (WGS)

Whole genome sequencing will be performed at the CCG (WGGC). In brief, for whole genome sequencing, the library will be prepared and size selected by using the CCG PCD free inhouse protocol based on Illumina® TruSeq® DNA Sample Preparation Kit and Agencourt AMPure XP beads, starting with 1,2 µg genomic DNA followed by one cycle of PCR to complete adapter structure. The library will be validated with the Agilent 2200 TapeStation and quantified by qPCR. For sequence analyses, the Illumina NovaSeq 6000 platform (Illumina, San Diego, USA) will be used. We calculate with 120 GB of sequence data and average coverage of 30-40-fold. Paired-end reads generated from sequencing will be mapped to the hg19 reference genome using BWA-ALN (version 0.6.2). After mapping, duplicates will be marked using Picard (version 1.64; http://picard.sourceforge.net) and basecalling quality score recalibration and local indel realignment will be performed using GATK (version 1.6.11). Enrichment statistics will be computed by Picard on the resulting BAM. Variants will be called genome wide using samtools mpileup (version 0.1.18) and in the complete target region using GATK UnifiedGenotyper (version 1.6.11). The resulting variants will be annotated with software developed at the CCG based on the ENSEMBL b68 gene models and filtered to exclude variants of low confidence (alternative allele frequency <10%, number of reads at variant position <5, variant quality score <10, number of reads supporting the variant <3). The remaining variants will be annotated with their presence in public databases (dbSNP, 1000 Genomes Project, Exome Variant Server (EVS http://evs.gs.washington.edu/EVS/), dbVAR and DGVa, GERP, ENSEMBL, and the commercial HGMD professional database) as well as a CCG inhouse exome collection. Effects on splicing will be predicted using the maximum entropy approach from Yeo and Burgeand SIFT, POLYPHEN, and RVIS scores for all coding

variants will be taken into account. The GATK UnifiedGenotyper variant list will be used to compute regions of homozygosity with Allegro. The annotated variant lists will be uploaded to the CCG's varbank (https://varbank.ccg.uni-koeln.de) and Varbank Version 2 (https://varbank.ccg.uni-koeln.de/varbank2/#undefined) database for further evaluation.

Supplementary Table S1. Overview of the diagnostic PCD-gene panel. Genes included in the gene panel related to ciliary motility, PCD and laterality defects.

Gene	Locus	References
DNAH9	**17p12**	**4,5**
DNAH5	**5p15**	**6**
DNAH11	**7p15.3**	**7,8**
DNAI1	**9p13.3**	**9,10**
DNAI2	**17q25.1**	**11**
TXNDC3/NME8	**7p14.1**	**12**
DNAL1	**14q24.3**	**13**
CCDC103	**17q12**	**14**
CCDC114/ODAD1	**19q13.33**	**15,16**
ARMC4/ODAD2	**10p21**	**17**
CCDC151/ODAD3	**19p13.2**	**18**
TTC25/ODAD4	**17q21.2**	**19**
LRRC56/DNAAF12	**11p15.5**	**20**
LRRC50/DNAAF1	**16q24**	**21,22**
KTU/DNAAF2	**14q21.3**	**23**
DNAAF3	**19q13**	**24**
DYX1C1/DNAAF4	**15q21**	**1**
SPAG1	**8q22**	**25**
ZMYND10/DNAAF7	**3p21.3**	**26,27**
HEATR2/DNAAF5	**7p22.3**	**28**
C21ORF59/CFAP298	**21q22.1**	**29**
LRRC6/DNAAF11	**8q24**	**30,31**
PIH1D3/DNAAF6	**Xq22.3**	**32,33**
C11ORF70/CFAP300	**11q22.1**	**34,35**

RPGR	**Xp21.1**	**36**
OFD1	**Xp22**	**37**
CFAP57	**1p34.2**	**38**
HYDIN	**16q22**	**39**
SPEF2	**5p13.2**	**40**
STK36	**2q35**	**41**
CFAP74	**1p36.33**	**42**
CFAP221	**2q14.2**	**43**
RSPH1	**21q22.3**	**44,45**
RSPH9	**6p21**	**46**
RSPH4A	**6q22**	**46**
RSPH3	**6q25.3**	**47**
DNAJB13	**11q13.4**	**48**
CCDC164/DRC1	**2p23**	**49**
CCDC65/DRC2	**12q13.12**	**29,50**
GAS8/DRC4	**16q24.3**	**51**
CCDC39	**3q26**	**52**
CCDC40	**17q25**	**53**
CCNO	**5q11.2**	**54**
MCIDAS	**5q11.2**	**55**
FOXJ1	**17q25.1**	**56**
TP73	**1p36.32**	**57**
CCDC11	**18q21.1**	**58**
ENKUR	**10p12.1**	**59**
GAS2L2	**17q12**	**60**
NEK10	**3p24.1**	**61**
TTC12	**11q23.2**	**62**

Nasal Nitric Oxide Measurements

During an exhalation-against-resistance maneuver (velum closure technique), nasal nitric oxide (NO) production rate was measured as described previously [63] using the chemiluminescence NO analyzers EcoMedics CLD88 (Duernten) or Niox Flex (Aerocrine). In individuals below 6 years of age nasal NO production rate was measured during normal tidal breathing without velum closure.

High-speed video microscopy analyses (HVMA)

Respiratory epithelial cells from nasal brush biopsies were analyzed with a Zeiss AxioVert A1 microscope (40x and 63x phase-contrast objective lens) equipped with a Basler sc640-120fm monochrome high-speed video camera (Basler) set at 120 frames per second. Two female and two male healthy controls were included in the HVMA analyses. Ciliary beat frequency and pattern was assessed with the SAVA system [64]. The ciliary beat pattern was evaluated on slow-motion playbacks as described previously [65].

Pulmonary Radioaerosol Mucociliary Clearance (PRMC) measurements for *in vivo* radiolabeled tracer whole lung retention studies

PRMC measurement was performed as previously described [66,67]. In short, insoluble Technetium ^{99m}Tc labelled nano-colloids were aerosolized and inhaled by 20 slow inspirations and successive forced expirations. Initial lung deposition and subsequent pulmonary mucociliary clearance immediately after inhalation of the radiolabeled tracer were assessed by repeated dynamic and static scintigraphic acquisitions for 2 hours. In addition, a static measurement after 24 hours and a Krypton ^{81m}Kr ventilation image of the ventilated lung area was performed. Whole-lung retention after 1 hour (LR1) and 2 hours (LR2) after tracer inhalation were compared to predicted values calculated from penetration index, age and sex using own reference equations [68]. Tracheobronchial velocity (TBV, bolus transport) was measured from dynamic acquisitions within the first hour. Involuntary cough was monitored by trained staff and significant coughing would render the test inconclusive to avoid false positive PRMA results due to cough clearance. If a subject coughed during the test, voluntary cough clearance was assessed by 1min of rigorous coughing after 2h by analyzing both the central part and the total lung regions [69]. Nasal Mucociliary Clearance (NMC) velocity was further assessed in one subject (1) by a 20min dynamic acquisition performed after administration of one drop ^{99m}Tc-albumin colloid tracer applied by a Hamilton syringe to the nasal concha media [70]. In non-PCD controls median TBV (IQR;range) was 4 (3.8 – 5.7; 2.0 – 6.0) mm/min [69,70].

High-resolution Immunofluorescence Microscopy

High-resolution immunofluorescence (IF) microscopy of respiratory epithelial cells was performed as previously described [1,71,72] using antibodies directed against the ODA components DNAH5, DNAH9, DNAI1 and DNAI2 and the IDA component DNALI1. For co-staining with the monoclonal anti-DNAH5 antibody, polyclonal antibodies directed against GAS8 was used (HPA041311, Sigma) as ciliary marker. For co-stainings with polyclonal antibodies (anti-DNALI1, -DNAI1, -DNAI2, -DNAH5, -DNAH9) a monoclonal antibody directed against acetylated tubulin was used (T6793, Sigma). For male (n=1) and female (n=2) controls, OP-1796 I2, OP-1796 II1, OP-1826 I2, OP-1826 II1, OP-3577 I2, OP-3577 II1 a total of 500 cells per IF staining were counted. For OP-2835 II1, 200 cells and for OP-2835 I2 and OP-2835 II2 a total of 75 cells per IF staining and individual were counted. High-resolution fluorescence images were taken using a Zeiss Apotome Axiovert 200 (processed with AxioVision 4.8) or Zeiss laser scanning microscope LSM880 (processed with ZEN2 software). Figures were prepared with Adobe Creative Suite 4.

Immunoblotting

Proteins were extracted from nasal epithelial cells of healthy controls (female; n=2) and individuals carrying hetero- and hemizygous pathogenic variants in *DNAAF6* cultured under ALI-conditions after complete differentiation using the following buffer: 50 mM Tris-HCl (pH 8.0), 150 mM NaCl, 1% IGEPAL, 10% Glycerol, and 0.5 mM EDTA supplemented with cOmplete™ Mini EDTA-free Protease Inhibitor Cocktail Tablets (Roche) and Phosphatase Inhibitor Cocktails 2 and 3 (Sigma-Aldrich). Using the Mikro-Dismembrator U (Sartorius), cell lysates were homogenized (2,000rpm, 3min) and proteins were separated from residual cell components by a final centrifugation step (11,500rpm; 20min; 4°C). To gauge the protein content of the cell lysate, proteins were separated in a NuPAGE® 4- 12 % Bis-Tris gel (Invitrogen) and stained by silver staining using the Proteo SilverTM Silver Stain kit (Prot-SIL1, Sigma) according to the manufacture's protocol. For immunoblotting, proteins were electrophoresed in a NuPAGE® 4-12% Bis-Tris gel and transferred to an Invitrolon™ polyvinylidene difluoride (PVDF)-membrane (novex® by life technologies). PVDF-membrane was washed two times (5 min each) with Tris-buffered saline plus Tween 20 (1xTBST) and blocked in 5 % BSA in 1xTBST for 120min at room temparature. The rabbit polyclonal primary antibodies directed against DNAAF6 (1:1000; HPA072496) and GAPDH (1:1000; Cell Signaling, #2118) were diluted in 1x TBST incubated overnight at 4°C. After washing with 1xTBST four times (7.5 min each) at room temperature, the membrane was incubated with secondary donkey anti-rabbit HRP antibody (1:3,000 diluted in 1xTBST; NA934V, GE Healthcare) for 60min at room temperature. The membrane was washed additional four times (7.5 min. each) with 1xTBST before performing the enhanced chemoluminescence (ECL) step

using Prime Western Blotting Detection Reagent (GE Healthcare). Digital images were acquired using a FUSION-SL Advance Imager (PeqLab). the Contrast of the images was optimized using Adobe Photoshop CS4 (Adobe),

Transmission electron microscopy

Transmission electron microscopy was performed as previously described [73]. In total, 431 ciliary cross-sections of three healthy individuals (male (n=1) and female (n=2)) and 581 cross-sections from OP-1796 I3 were analyzed.

Cell Culture of Primary Respiratory Epithelial Cells in Air-liquid Interface Culture

Human nasal ciliated epithelial cells of healthy controls (hRECs), female carriers and PCD individuals were obtained by nasal brush biopsy, resuspended in DMEM/Ham´s F12 (1:1) (Invitrogen, Karlsruhe, Germany) supplemented with 2 % UltroserG (Pall Life Sciences, Germany) and Antibiotic-Antimycotic (100 x) (Invitrogen, Karlsruhe, Germany), plated on collagen-coated tissue flasks and cultured in a humidified atmosphere with 5 % CO2 at 37 °C. Medium was replaced three times per week until 70 – 80 % confluence was reached. Then hRECs were treated with collagenase type IV (200 U/mL; Worthington Biochemical Corporation, St. Katharinen, Germany) and were trypsinized for 5 min in 1x Trypsin-EDTA Solution (Sigma-Aldrich Co. LLC, St. Louis, USA). Cell pellet was resuspended in B-ALI Growth Basal Medium (Lonza Cologne GmbH, Germany) and seeded onto collagen coated transwell inserts (100.000 cells per insert; Costar™ Corning® 3470 Transwell™ Clear Polyester Membrane Inserts For 24-Well Plates, Corning Incorporated, USA). Cells were cultured with 5 % CO_2 at 37 °C in a humidified atmosphere and fed with B-ALI Growth Basal Medium from the basolateral and apical compartment every day. Once confluency was reached, airlift was performed by removing the apical medium and replacing the basal medium by B-ALI differentiation medium. Medium was changed three times per week until further experiments were performed.

***In vitro* Ciliary Clearance Assay using immunofluorescent labeled particles**

Human nasal ciliated epithelial cells cultured under ALI-conditions were used for tracking experiments. In total, three ALI-Transwell® inserts per person were tracked at day 30 after airlift. Particle transport was measured in 18 healthy female individuals and one healthy male individual (age 25-60 years). First, secreted mucus was removed by washing the apical compartment with Dulbecco's Phosphate-Buffered Saline (DPBS; without Mg^{2+}/Ca^{2+}). In a second step cultures were equilibrated for 20min on the heating plate (37°C) of a Nikon Eclipse

Ti-S microscope. Afterwards, 100µl cell culture medium was added to the apical compartment of the Transwell® inserts for 10min on the heating plate (37°C). 10µl of a fluorescent beads stock solution (FluoSpheres® 0.5 and 2.0µm in diameter; Thermo Fisher, diluted 1:1,000 in DPBS without Mg^{2+}/Ca^{2+}) were mixed with 90µl pre-warmed cell culture medium and added to the apical compartment of the Transwell® insert as well. Transport of fluorescent nanoparticles by ciliary beating was recorded using the Nikon Eclips Ti-S microscope (20x objective lens) equipped with the NIS-Elements Advanced Research software (20 sec; 7.5 frames per second). Nanoparticles were excited with a wavelength of 546nm (100ms exposure time). Tracking videos were evaluated using the NIS-Elements Advanced Research software (Version 4.51.000) and NIS Advanced 2D Tracking plug-in to generate polar graphs and to determine the speed (µm/s). The significantly reduced particle transport measured in the male PCD individuals is a thermal driven background flow (Brownian movement). In total, 30 videos per individuals were analyzed for statistical evaluation and thereby 253 particles were tracked per video on average from three different cell culture inserts from each individual. As two different bead sizes (0.5µm and 2µm) were used for the analyses, values were normalized against the mean value of the healthy control group. Z-stack projections of movies were generated using ImageJ. In parallel to each recorded tracking video, a corresponding differential interference contrast (DIC) video was taken by an additionally equipped Basler sc640-120fm monochrome high-speed video camera (recording 125 frames per second) to state the cells condition as well as the ciliary beating pattern. DIC videos were evaluated using SAVA software [64].

Statistical analyses

Statistical analyses were performed using R, GraphPad Prism 9.0.2, the ANOVA-two-tailed test and student's t-test.

Supplementary Results

Mutational Analysis and Family History

All genetic variants identified in *DNAAF6* were classified as pathogenic (class 5) according to ACMG/AMG criteria [2]. Thus, we only include individuals with a certain genetic diagnosis warranting no other test.

To detect the disease-causing variants in the PCD affected male individuals OP-1796II1 and OP-1826II1 (Figure2A) we performed WES and Sanger sequencing of all *DNAAF6* exons. Using WES, we did not identify any disease-causing variant in *DNAAF6*, because WES does not cover sequence analyses of the untranslated first exon of *DNAAF6*

(Figure 2). Amplification of all *DNAAF6* exons including the splice sites and the untranslated first exon led to the identification of a hemizygous deletion of the 5' region deleting the first untranslated exon. Subsequent breakpoint analysis revealed a 28kb deletion also affecting the untranslated first exons of *NUP62CL* (Figure2A, Supplementary Figure1). Thus, we found evidence for a contiguous gene deletion syndrome involving also *NUP62CL*. To date, no disease-causing variants have been reported in *NUP62CL*. Segregation analyses in the female individuals OP-1826I2, OP-1796I2 and OP-1796I3 showed that they are heterozygous carriers of the 28kb deletion and that OP-1796II1 and OP-1826II1 have inherited the hemizygous 28kb deletion (Supplementary Figure1). Additionally, we received blood samples from the father (OP-1796I1) and twin sisters (OP-1796II2 and OP-1796II3). All three individuals did not carry the 28kb deletion involving *DNAAF6*.

Targeted gene panel sequencing of PCD individual OP-3577II1 revealed a hemizygous 10.6kb deletion comprising *DNAAF6* exons 2-4 (Figure2B, Supplementary Figure1). Segregation analyses revealed that the mother OP-3577I2 also carries the deletion, but not her brother (OP-3577I3) or the grandmother (OP-357702) (Figure2B, Supplementary Figure2), indicating that this is a *de novo* mutation occurring first in OP-3577I2. OP-3577I2 reported difficulties to get pregnant and had one miscarriage (spontaneous abortion in the sixth week of pregnancy) in the past. OP-3577I2 gave birth to another son (OP-3577II2) who did not inherit the 10.6kb deletion (Supplementary Figure2).

Analyses of the pedigree and family history of OP-3141II1 indicated X-linked inheritance pattern of a PCD variant causative for ODA and IDA defects consistent with a *DNAAF6* defect. Therefore, we amplified all seven exons of *DNAAF6* and identified a complete hemizygous deletion including all exons of *DNAAF6* in individual OP-3141II1. Whole genome sequencing was used to further delineate the boundaries of the deletion, which has a size of approximately 400kb also comprising the adjacent genes *RBM41* and *NUP62CL* (Figure2C,Supplementary Figure3). Thus, we found evidence for another gene deletion syndrome also involving three genes including *DNAAF6*. Like in *NUP62CL* also in *RBM41,* no disease-causing variants are reported so far. Thus, both genes possibly are dispensable for humans. OP-3141II1 is the fourth of six children. He has three older and one younger sister (Figure2C). The only brother was mature born, but died ten days after birth due to cardiorespiratory failure of unknown cause. His oldest sister gave birth to two male individuals: The first-born died three months after birth; the second-born died four months after birth. Both died of unknown causes with cardiorespiratory failure. With another partner, she gave birth to another boy, which is healthy. The second oldest sister has three healthy children, two girls and a boy. The third oldest sister gave birth to a healthy boy. The younger sister has no children. The mother of the patient was reported to have a bronchial asthma. The father died

of a heart attack. Unfortunately, blood samples from additional family members were not available.

Targeted PCD gene panel sequencing of PCD individual OP-2835II1 identified the hemizygous pathogenic variant c.266G>A in *DNAAF6* (exon4) predicting premature stop of translation (p.Trp89*) (Figure2D, Supplementary Figure4). Segregation analyses revealed that the mother (OP-2835I2) and the grandmother (OP-283502) carry the variant in a heterozygous status whereas the father (OP-2835I1) is unaffected (Supplementary Figure4). The great-grandmother of OP-2835II1 died due to complications of an ectopic pregnancy (Figure2D). Before that, she had a spontaneous abortion and another child OP-283502 carrying the *DNAAF6* variant. OP-283502 gave birth to three daughters. The oldest sister has two healthy children, a girl, who already has another healthy daughter, and a boy. The second oldest sister, OP-2835I2 is carrier of the *DNAAF6* variant c.266G>A and has two children (Figure2D). She had one ectopic pregnancy with a previous partner. With her current partner, she had two spontaneous abortions and an ectopic pregnancy. They finally got one girl (OP-2835II2), who was her fourth pregnancy and who is a carrier of the *DNAAF6*-variant c.266G>A. In addition, she gave birth to the index PCD male individual OP-2835II1, who carries the hemizygous *DNAAF6*-variant c.266G>A. The younger sister had one abortion and no children (Figure2D, Supplementary Figure4).

Clinical Findings

As expected, all five males (age range 3 to 67 years of age) with hemizygous pathogenic *DNAAF6* variants displayed typical clinical symptoms and diagnostic findings consistent with PCD (Table 1). Three of the five (60%) individuals reported neonatal respiratory distress. All of the individuals reported a chronic wet cough and exhibited symptoms from chronic upper and lower airway disease, including chronic bronchitis. Additionally, four of five individuals (80%) reported bronchiectasis. Three of four analyzed males (75%) presented with reduced lung function (FEV1%pred.) and variable degree of obstruction (Table 1). Nasal NO production rates in all individuals were below the current cut-off value of 77nl/min. The adult male OP-3141 II1 did not father a child. He received andrological work-up, which revealed infertility due complete immotile sperm cells.

Our genetic analyses identified seven females (age range 26 to 67 years age) with heterozygous pathogenic variants available for detailed analyses (Table 1). None of the six studied females reported neonatal respiratory distress, bronchiectasis or chronic wet cough. However, intermittent wet cough was reported by OP-1796I3, and chronic otitis media was reported by OP-2835II2. Chronic sinusitis was reported in two individuals (OP-2835II2; OP-3577I2). Chronic bronchitis during childhood was reported in OP-2835II2. Recurrent pneumonia was observed in OP-1796I3. However, lung function testing was normal in all

tested individuals. Except OP-1796I2 showed subtle degree of obstruction (FEV1%pred. 77%) at the age of 43 years. Thus, the six studied females displayed either no or only subtle respiratory symptoms.

Immunoblotting

We performed immunoblot analyses using lysates from healthy control individuals, male PCD individuals OP-1796 II1, OP-1826 II1 and OP-3141 II1 and from the female carriers OP-3577 I1 and OP-1796 I3. Consistent with the pathogenic variants identified in *DNAAF6*, all analyzed PCD individuals showed absence of DNAAF6 (supplementary figure 17). Interestingly, we could observe a reduction of DNAAF6 in the analyzed female carriers, consistent with random X-chromosome inactivation (supplementary figure 17).

Supplementary Tables

Supplementary Table S2. Quantification of the overall ciliary motility observed by high-speed video microscopy in nasal respiratory ciliated cells (brushing and/or ALI culture) in female (n=2) and male (n=2) healthy controls, male PCD individuals OP-3577 II1, OP-1826 II1 and OP-3141 II1 carrying hemizygous pathogenic variants in *DNAAF6* and the female heterozygous carrier OP-1796 I3.

	After nasal brushing			After ALI culture		
	Cells with motile cilia	Cells with immotile cilia	Total number of cells	Cells with motile cilia	Cells with immotile cilia	Total number of cells
Male Healthy control (n=2)	59	0	59	108	2	110
Female Healthy control (n=2)	147	4	153	117	2	119
OP-1796 I3 (female carrier)	na			257	340	597
OP-1826 I2 (female carrier)	na			+	+	33
OP-2835 II2 (female carrier)	+	+	23	na		
OP-1796 II1 (hemizygous male)	na			0	+	5
OP-1826 II1 (hemizygous male)	na			0	538	538
OP-3141 II1 (hemizygous male)	na			0	205	205
OP-2835 II1 (hemizygous male)	0	+	6	na		
OP-3577 II1 (hemizygous male)	0	32	32	na		

Supplementary Table S3. Results of *in vivo* mucociliary clearance analysis. Lung retention compared to initial deposition at 0.5h, 1h, 2h and 24h. In non-PCD controls median (IQR;range) was 4 (3.8 – 5.7; 2.0–6.0) mm/min. LR: Lung retention; NA: Not applicable; TBV: Trachealbronchial velocity.

Subject	$LR_{0.5}$	LR_1 (z-score)	LR_2 (z-score)	LR_{24}	Bolus-transport (TBV) [mm/min]	Cough	Conclusion	Penetration index of aerosol	Voluntary cough clearance	Nasal Bolus-transport [mm/min]
OP-1796 II1 (hemizygous male)	96% (NA)	96% (1.9)	89% (1.8)	Abnormal	0	3 between 1 to 2 h	Abnormal	0.34	47%	0
OP-1796 I2 (heterozygous carrier)	86% (NA)	82% (0.9)	73% (0.6)	Normal	2.5	0	Normal	0.30	NA	NA
OP-1796 I3 (heterozygous carrier)	98% (NA)	96% (1.2)	89% (1.1)	Abnormal	1.7	0	Slightly abnormal	0.71	NA	NA
OP-1826 I2 (heterozygous carrier)	86% (NA)	74% (-0.6)	64% (-0.6)	Slightly abnormal in right lung	3.0	4 between 0 to 0.5 h	Slightly regional abnormal	0.54	0%	NA

Supplementary Figures

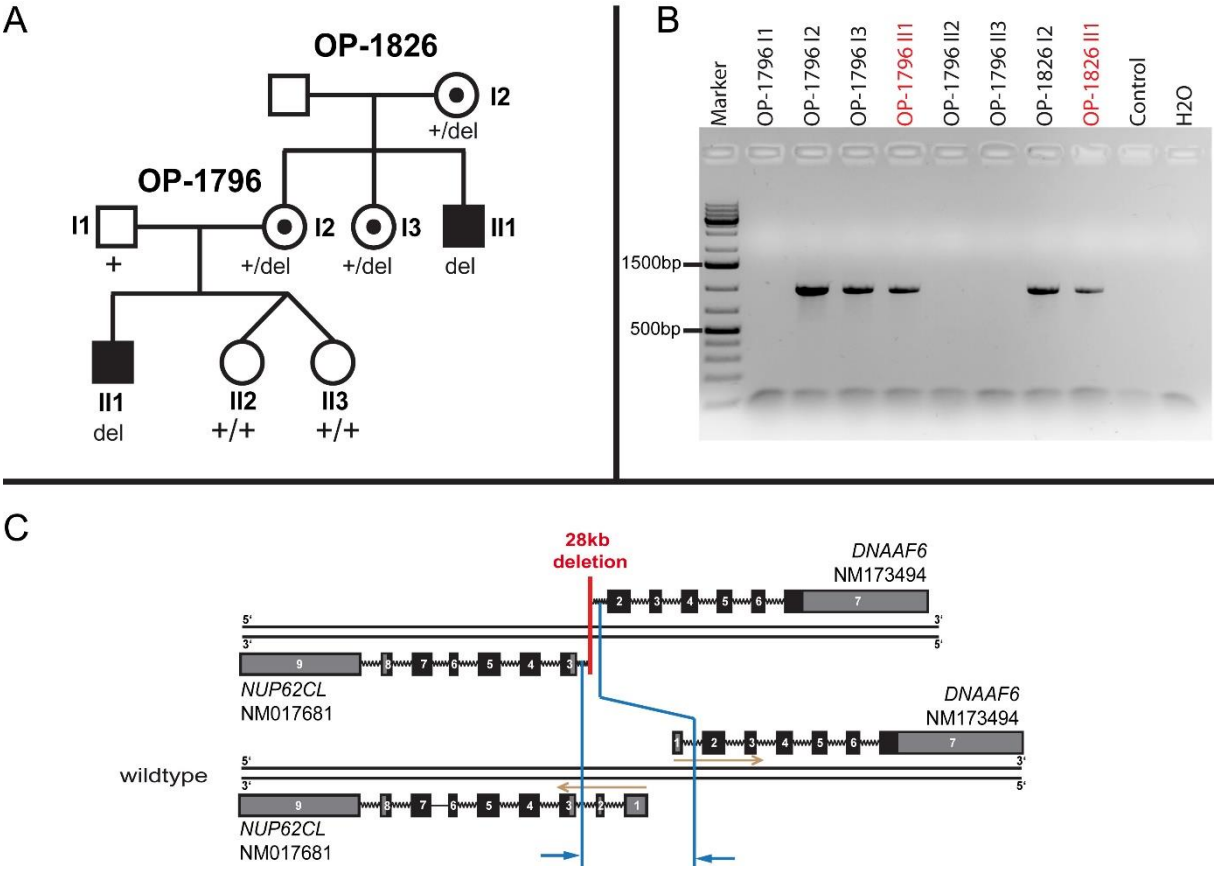

Supplementary Figure 1. In family OP-1826/OP-1796, a 28kb deletion including the first exon of *DNAAF6* and the first two exons of *NUP62CL* was identified. (A) Pedigree of family OP-1826/OP-1796. PCD-affected males are shaded black and unaffected siblings are shaded white. Heterozygous female carriers are indicated by a central dot. Genotypes are indicated in the pedigrees. (B) Breakpoint PCR showed that female individuals OP-1796 I2, OP-1796 I3, OP-1826 I2 and male PCD individuals OP-1796 II1 and OP-1826 II1 carry the 28kb deletion in *DNAAF6* and *NUP62CL.* (C) The identified 28kb deletion (red line) includes the first exon of *DNAAF6* and the first two exons of *NUP62CL.* The blue lines indicate the breakpoint PCR strategy.

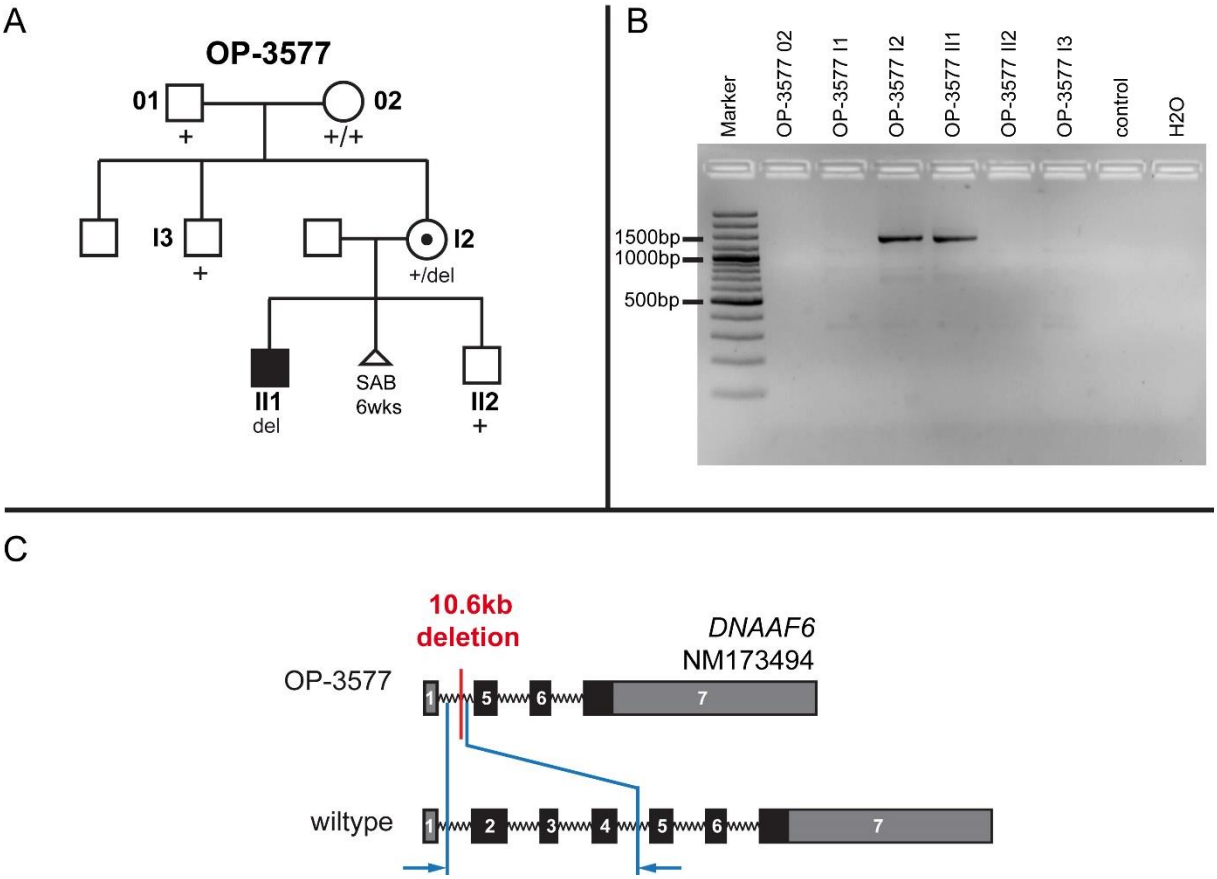

Supplementary Figure 2. In family OP-3577, a 10.6kb deletion was identified comprising *DNAAF6* exons 2, 3 and 4. (A) Pedigree of family OP-3577. The PCD-affected male is shaded black and unaffected siblings are shaded white. Heterozygous female carriers are indicated by a central dot. Genotypes are indicated in the pedigrees. (B) Breakpoint PCR showed that female individual OP-3577 I2 and male PCD individual OP-3577 II1 carry the 10.6kb deletion in *DNAAF6* but not her brother (OP-3577 I3) or the grandmother (OP-3577 02), indicating that this is a *de novo* variant occurring first in OP-3577 I2. (C) The identified 10.6kb deletion (red line) comprises *DNAAF6* exons 2, 3 and 4. The blue lines indicate the breakpoint PCR strategy. SAB: Spontaneous abortion; wks: Weeks.

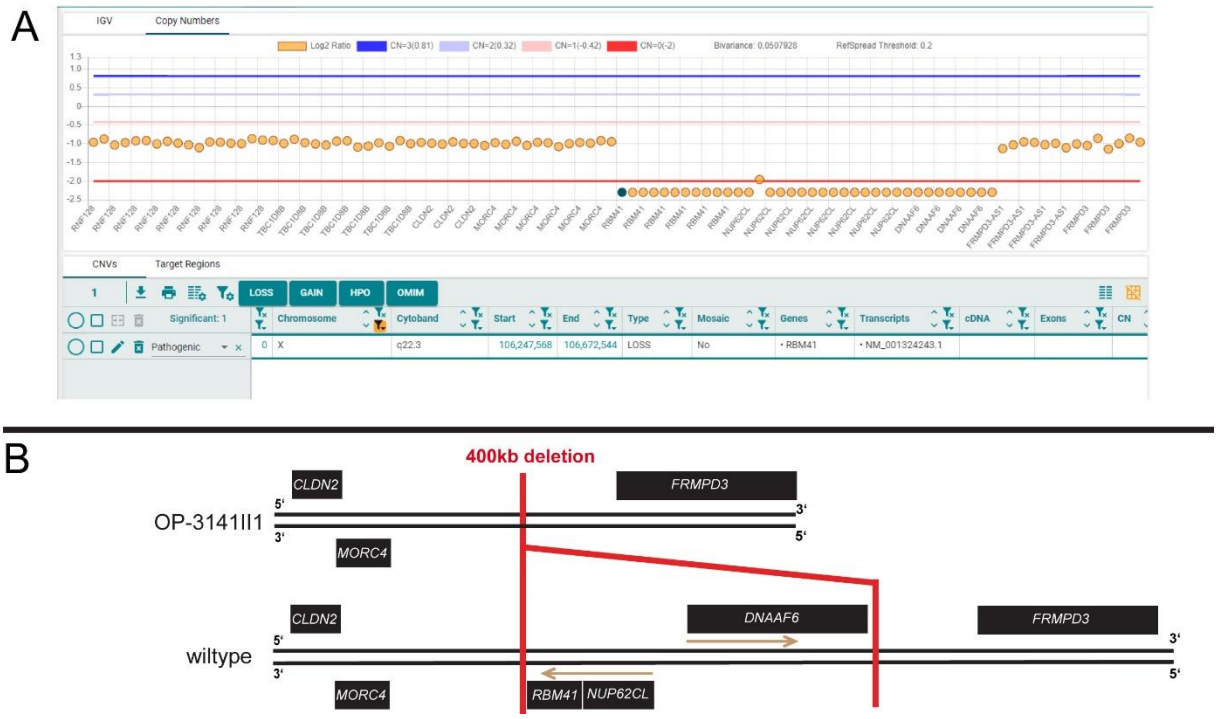

Supplementary Figure 3. A 400kb deletion was identified in OP-3141 II1 comprising *DNAAF6*, *NUP62CL* and *RBM41*. (A and B) Copy number variation analysis revealed an approx. 400kb large deletion (marked in red in B) comprising *DNAAF6*, *NUP62CL* and *RBM41* (B).

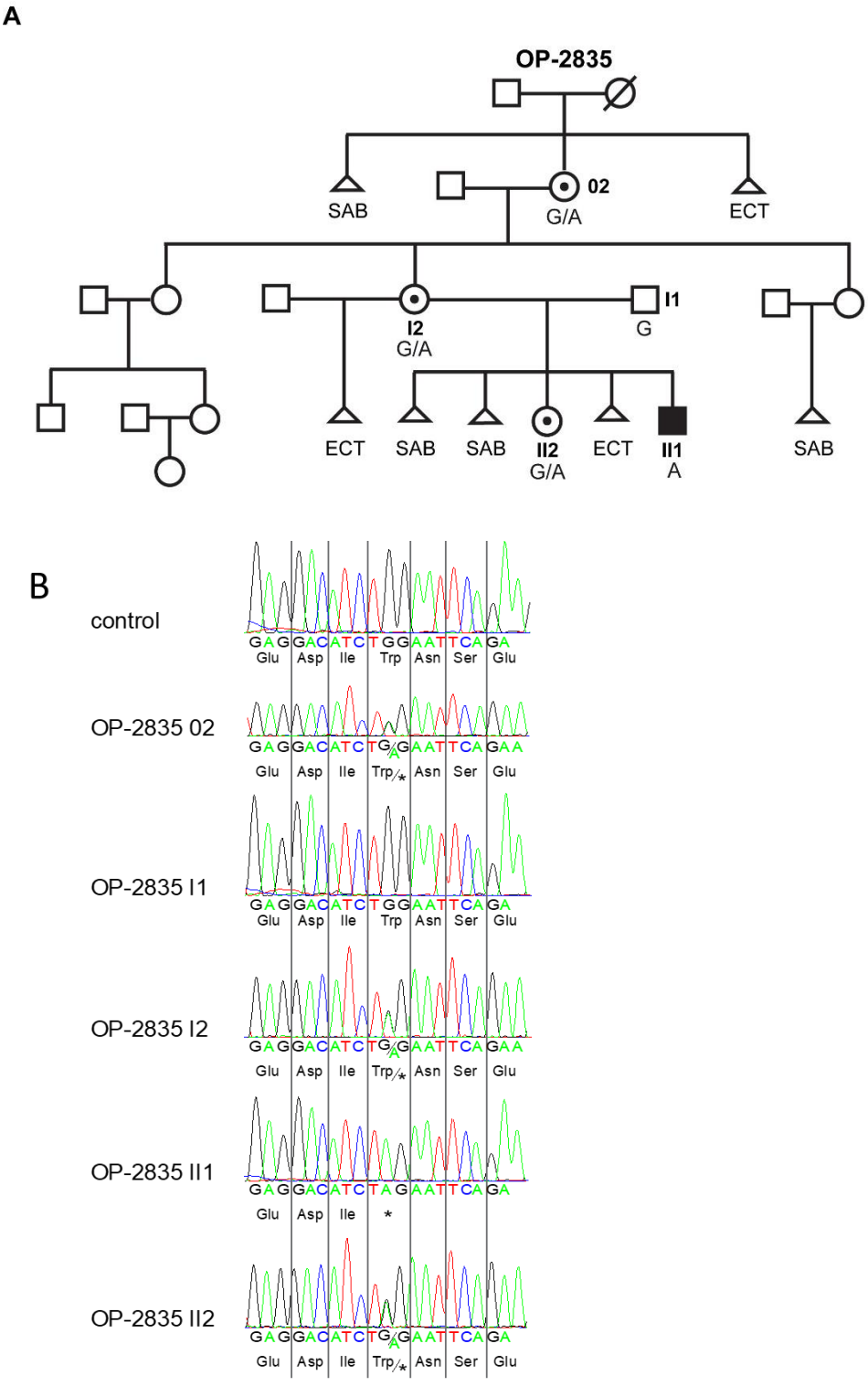

Supplementary Figure 4. Segregation analyses of the pathogenic variant c.266G>A (p.Trp89*) in *DNAAF6* identified in family OP-2835. (A) Pedigree of family OP-2835. PCD-affected males are shaded black and unaffected siblings are shaded white. Heterozygous female carriers are indicated by a central dot. Genotypes are indicated in the pedigrees. (B) Segregation analyses in family OP-2835 revealed that the mother (OP-2835 I2) and the grandmother (OP-2835 02) carry the variant in a heterozygous status whereas the father (OP-2835 I1) is unaffected. The asterix indicates stop of translation. ECT: Ectopic pregnancy; SAB: Spontaneous abortion.

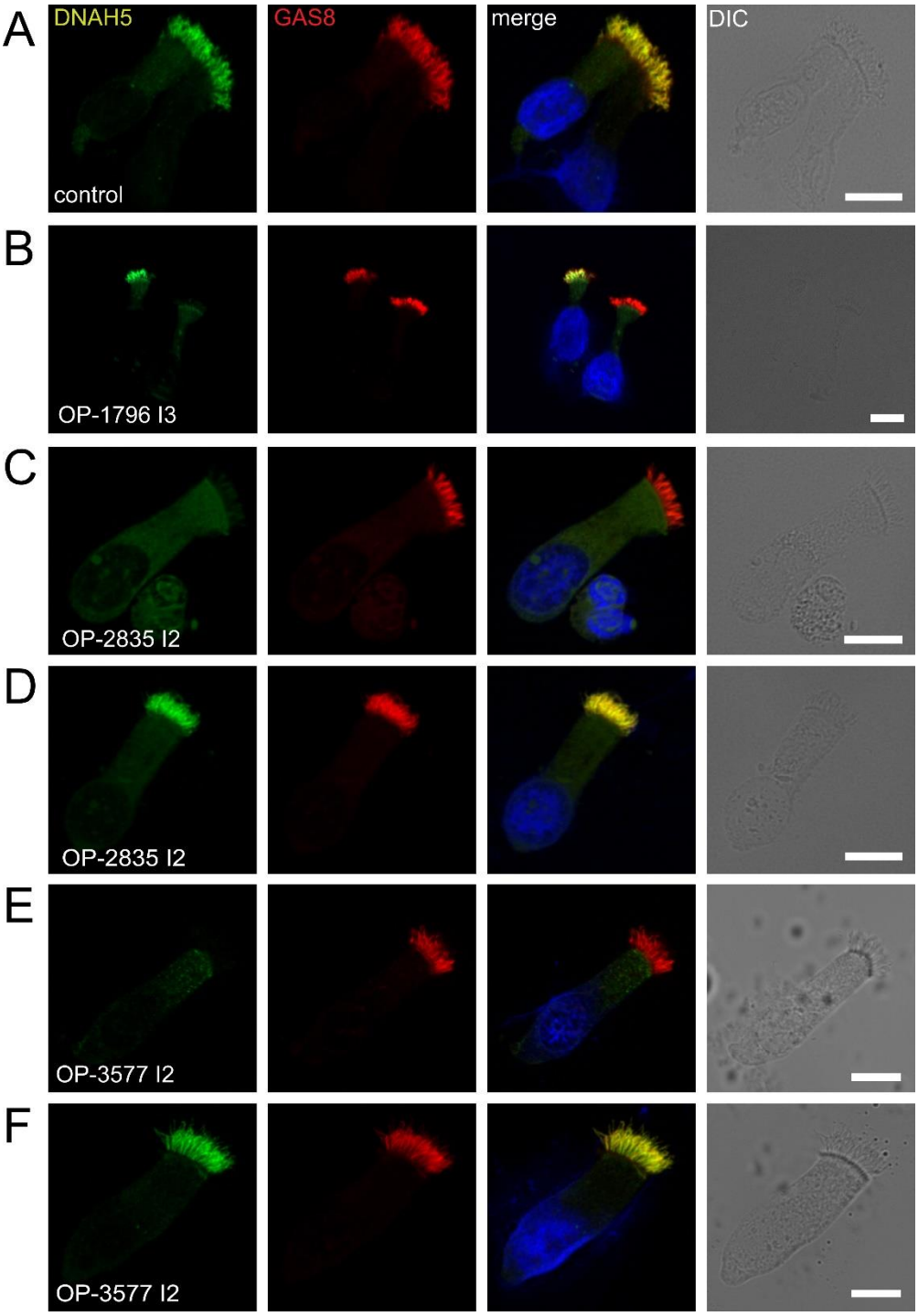

Supplementary Figure 5. Heterozygous *DNAAF6* pathogenic variants in females result in a mosaic of cells with and without axonemal outer dynein arm defects.
(A-E) Respiratory epithelial cells from female control individuals and females with heterozygous pathogenic *DNAAF6* variants were double-labeled with antibodies directed against the outer dynein arm protein DNAH5 (green) and GAS8 (red). Both proteins colocalize (yellow) along the ciliary axonemes in all cells from the unaffected control (A). In females with heterozygous *DNAAF6* pathogenic variants, DNAH5 was completely absent or severely reduced from the ciliary axonemes of some cells (B,C,D,F) or showed a normal localization in ciliary axonemes of other cells (B,C,E). Nuclei were stained with Hoechst33342 (blue). Scale bars represent 10µm.

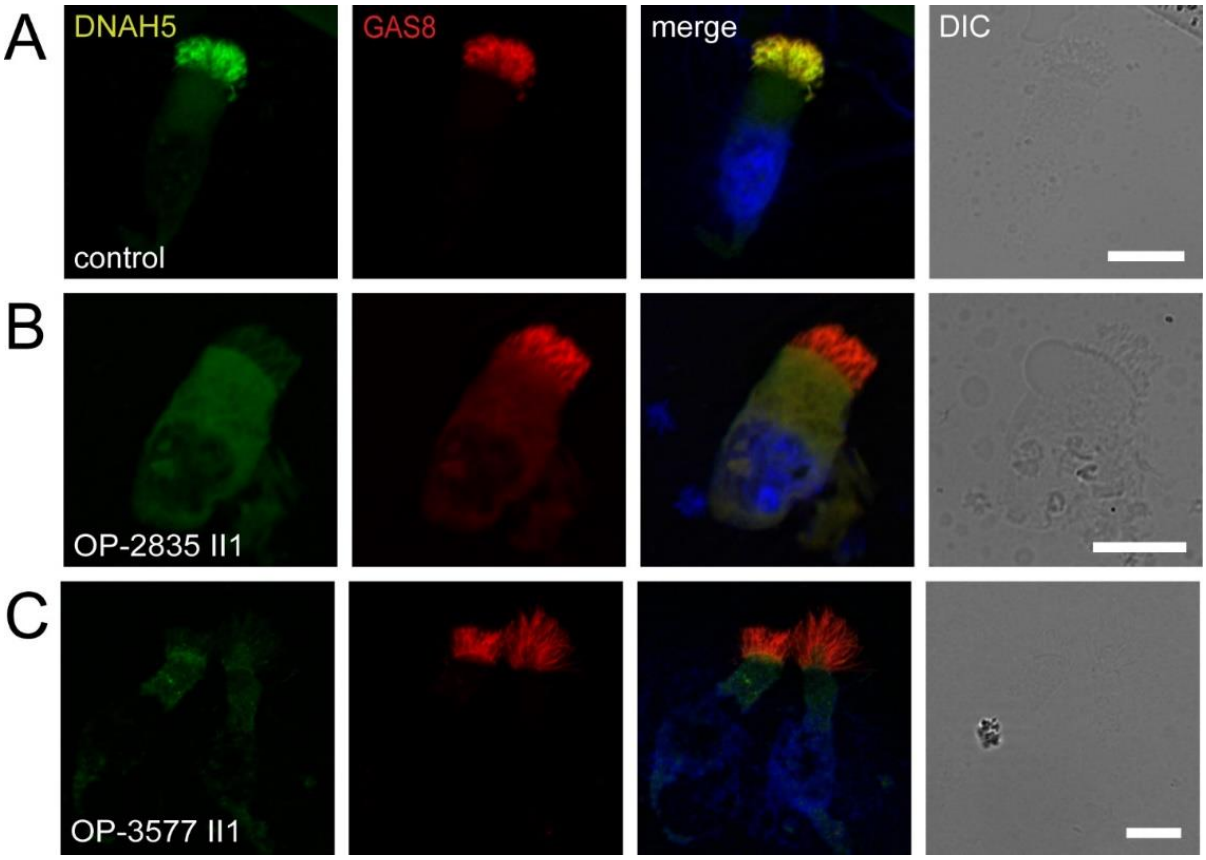

Supplementary Figure 6. Hemizygous pathogenic variants in *DNAAF6* result in outer dynein arm defects of PCD affected males. (A-C) Respiratory epithelial cells from control individuals and male PCD individuals with hemizygous pathogenic *DNAAF6* variants were double-labeled with antibodies directed against the outer dynein arm protein DNAH5 (green) and GAS8 (red). Both proteins colocalize (yellow) along the ciliary axonemes in cells from the unaffected control (A). In cells from PCD individuals OP-2835 II1 (B) and OP-3577 II1 (C), DNAH5 was completely absent or severely reduced from the ciliary axonemes of all cells analyzed. Nuclei were stained with Hoechst33342 (blue). Scale bars represent 10µm.

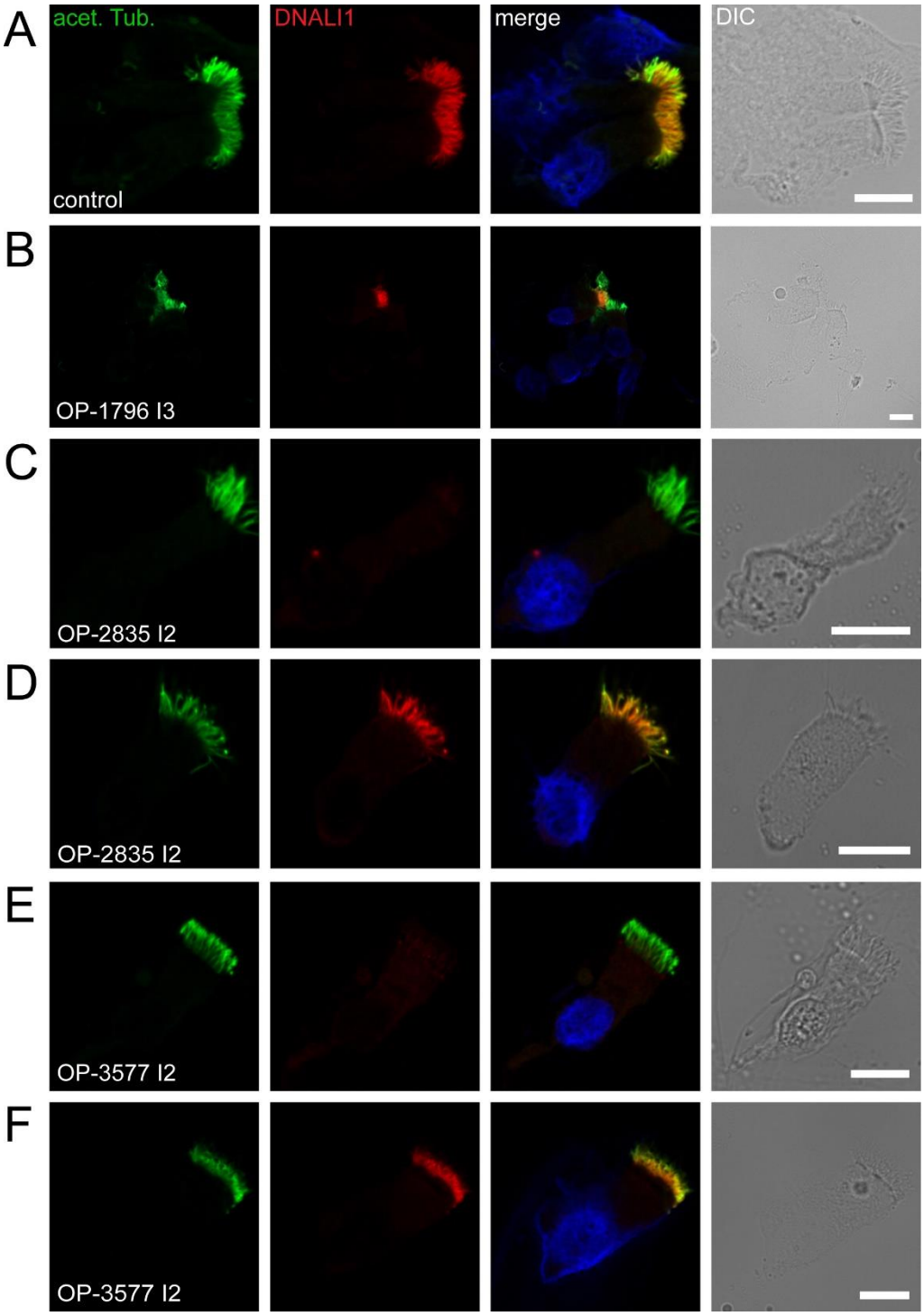

Supplementary Figure 7. Heterozygous *DNAAF6* pathogenic variants in females result in a mosaic of cells with and without axonemal inner dynein arm defects. (A-E) Respiratory epithelial cells from a female control and females with heterozygous pathogenic *DNAAF6* variants were double-labeled with antibodies directed against acetylated tubulin (green) and the inner dynein arm protein DNALI1 (red). Both proteins colocalize (yellow) along the ciliary axonemes in all cells from the unaffected control (A). In females individuals with heterozygous pathogenic *DNAAF6* variants DNALI1 was completely absent or severely reduced in the ciliary axonemes of some cells (B,C,E) or showed a normal localization in other cells (B,D,F). Nuclei were stained with Hoechst33342 (blue). Scale bars represent 10µm.

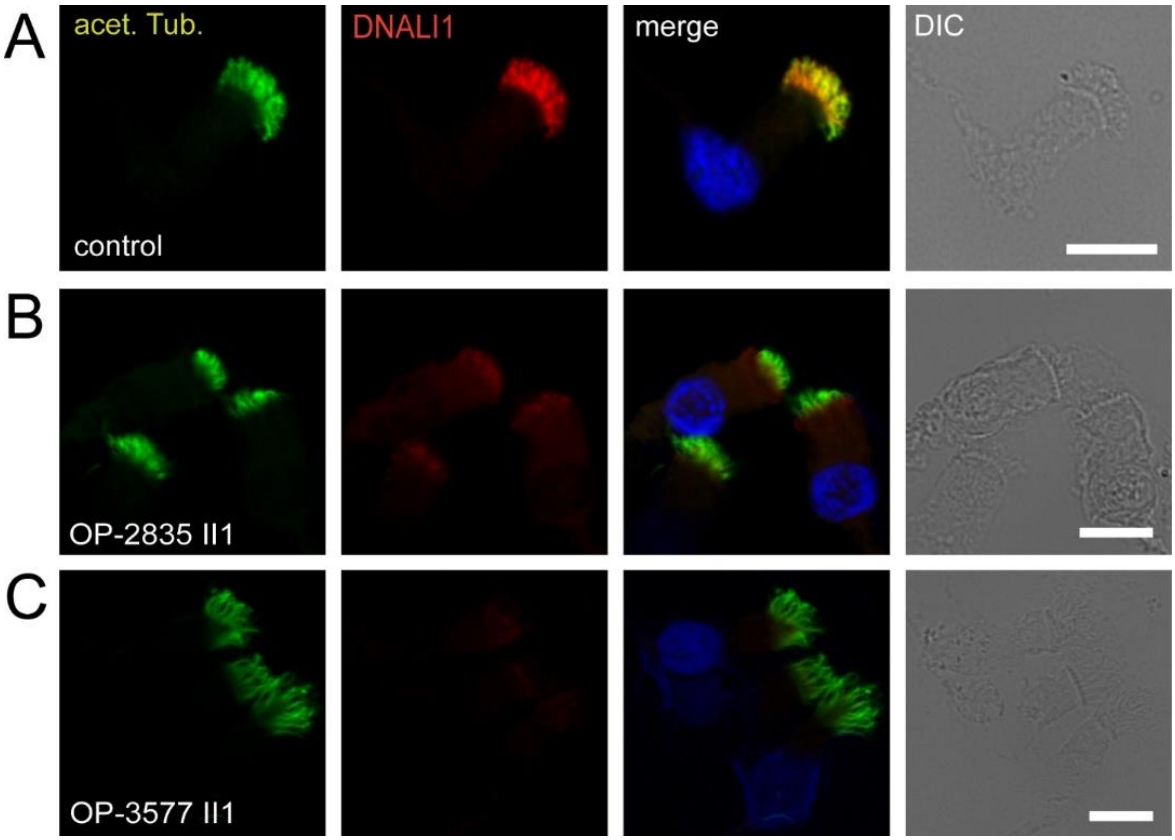

Supplementary Figure 8. Hemizygous pathogenic variants in *DNAAF6* result in outer and inner dynein arm defects of PCD affected males. (A-C) Respiratory epithelial cells from a control and male PCD individuals with hemizygous pathogenic *DNAAF6* variants were double-labeled with the antibodies directed against acetylated tubulin (green) and the inner dynein arm protein DNALI1 (red). Both proteins colocalize (yellow) along the ciliary axonemes in all cells from the unaffected control (A). In cells from the male PCD individuals OP-2835 II1 (B) and OP-3577 II1 (C), DNALI1 was completely absent or severely reduced in the ciliary axonemes of all cells analyzed. Nuclei were stained with Hoechst33342 (blue). Scale bars represent 10µm.

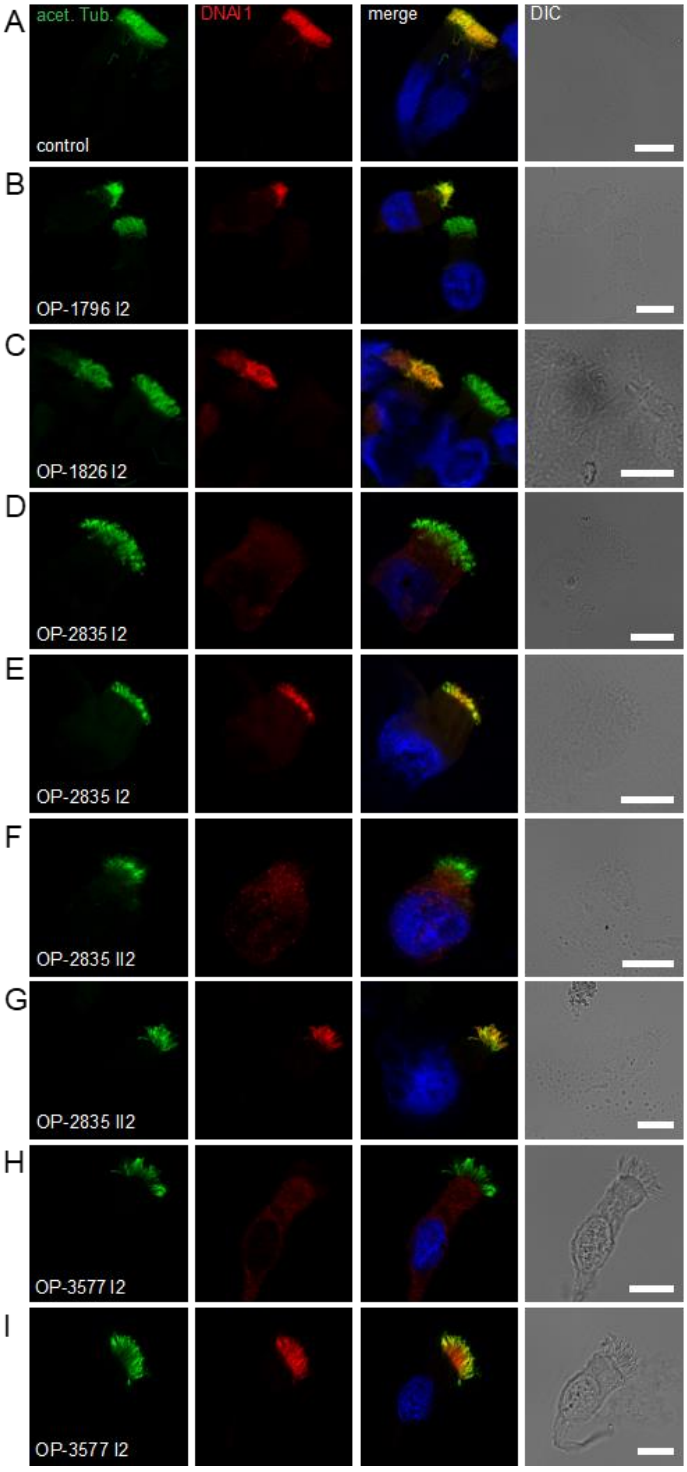

Supplementary Figure 9. Heterozygous *DNAAF6* pathogenic variants in females result in a mosaic of cells with and without axonemal outer dynein arm defects.
(A-I) Respiratory epithelial cells from female control individuals and females individuals with heterozygous pathogenic *DNAAF6* variants were double-labeled with antibodies directed against acetylated tubulin (green) and the outer dynein arm protein DNAI1 (red). Both proteins colocalize (yellow) along the ciliary axonemes in all cells from the unaffected control (A). In females with heterozygous *DNAAF6* pathogenic variants, DNAI1 was completely absent or severely reduced from the ciliary axonemes of some cells (B,C,D,F,H) or showed a normal localization in ciliary axonemes of other cells (B,C,E,G,I). Nuclei were stained with Hoechst33342 (blue). Scale bars represent 10µm.

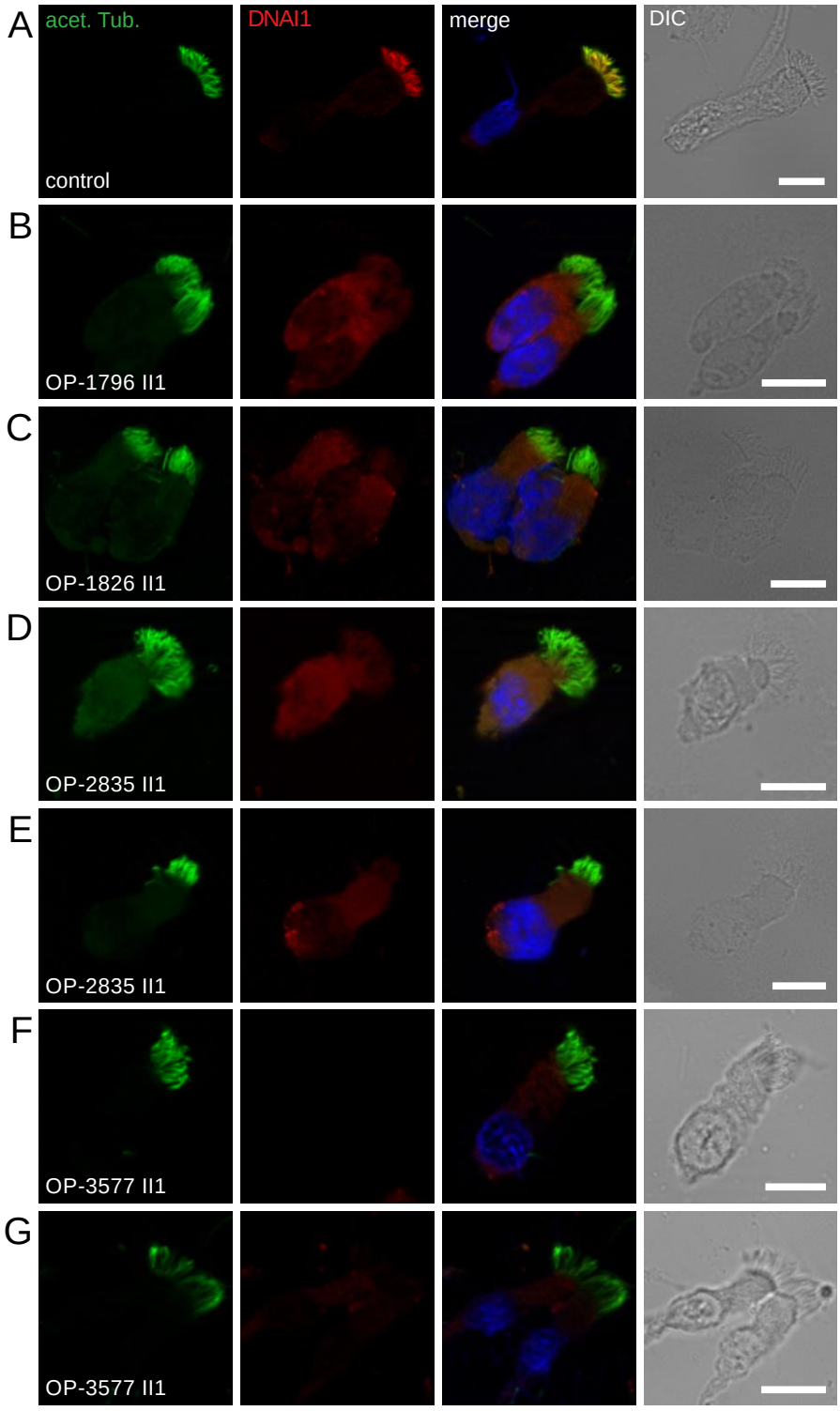

Supplementary Figure 10. Hemizygous pathogenic variants in *DNAAF6* result in outer dynein arm defects of PCD affected males. (A-G) Respiratory epithelial cells from control individuals and male PCD individuals with hemizygous pathogenic *DNAAF6* variants were double-labeled with antibodies directed against acetylated tubulin (green) and the outer dynein arm protein DNAI1 (red). Both proteins colocalize (yellow) along the ciliary axonemes in cells from the unaffected control (A). In cells from male PCD individuals OP1796 II1 (B), OP-1826 II1 (C), OP-2835 II1 (D,E) and OP-3577 II1 (F,G), DNAI1 was completely absent or severely reduced from the ciliary axonemes of all cells analyzed. Nuclei were stained with Hoechst33342 (blue). Scale bars represent 10µm.

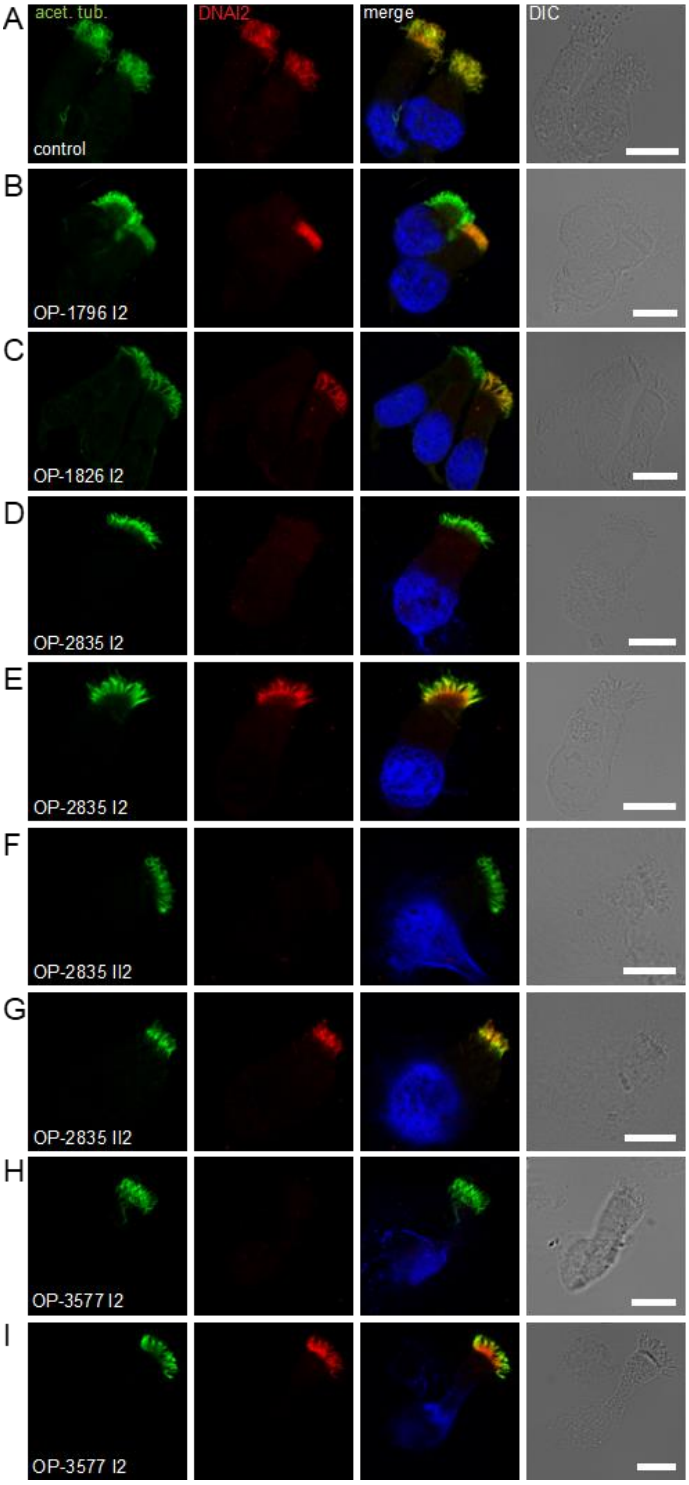

Supplementary Figure 11. Heterozygous *DNAAF6* pathogenic variants in females result in a mosaic of cells with and without axonemal outer dynein arm defects.
(A-I) Respiratory epithelial cells from female control individuals and females individuals with heterozygous pathogenic *DNAAF6* variants were double-labeled with antibodies directed against acetylated tubulin (green) and the outer dynein arm protein DNAI2 (red). Both proteins colocalize (yellow) along the ciliary axonemes in all cells from the unaffected control (A). In females with heterozygous *DNAAF6* pathogenic variants, DNAI2 was completely absent or severely reduced from the ciliary axonemes of some cells (B,C,D,F,H) or showed a normal localization in ciliary axonemes of other cells (B,C,E,G,I). Nuclei were stained with Hoechst33342 (blue). Scale bars represent 10µm.

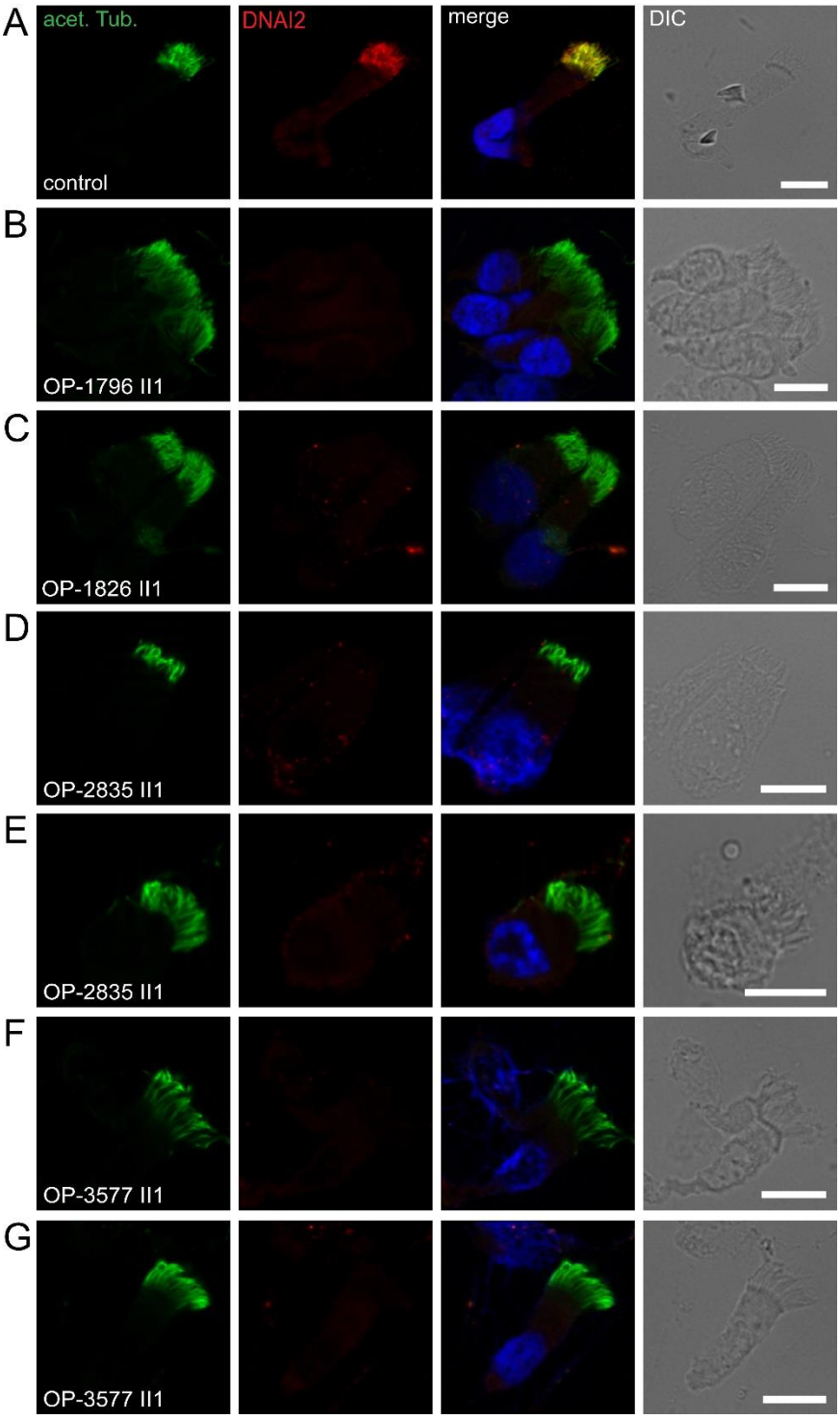

Supplementary Figure 12. Hemizygous pathogenic variants in *DNAAF6* result in outer dynein arm defects of PCD affected males. (A-G) Respiratory epithelial cells from control individuals and male PCD individuals with hemizygous pathogenic *DNAAF6* variants were double-labeled with antibodies directed against acetylated tubulin (green) and the outer dynein arm protein DNAI2 (red). Both proteins colocalize (yellow) along the ciliary axonemes in cells from the unaffected control (A). In cells from male PCD individuals OP1796 II1 (B), OP-1826 II1 (C), OP-2835 II1 (D,E) and OP-3577 II1 (F,G), DNAI2 was completely absent or severely reduced from the ciliary axonemes of all cells analyzed. Nuclei were stained with Hoechst33342 (blue). Scale bars represent 10µm.

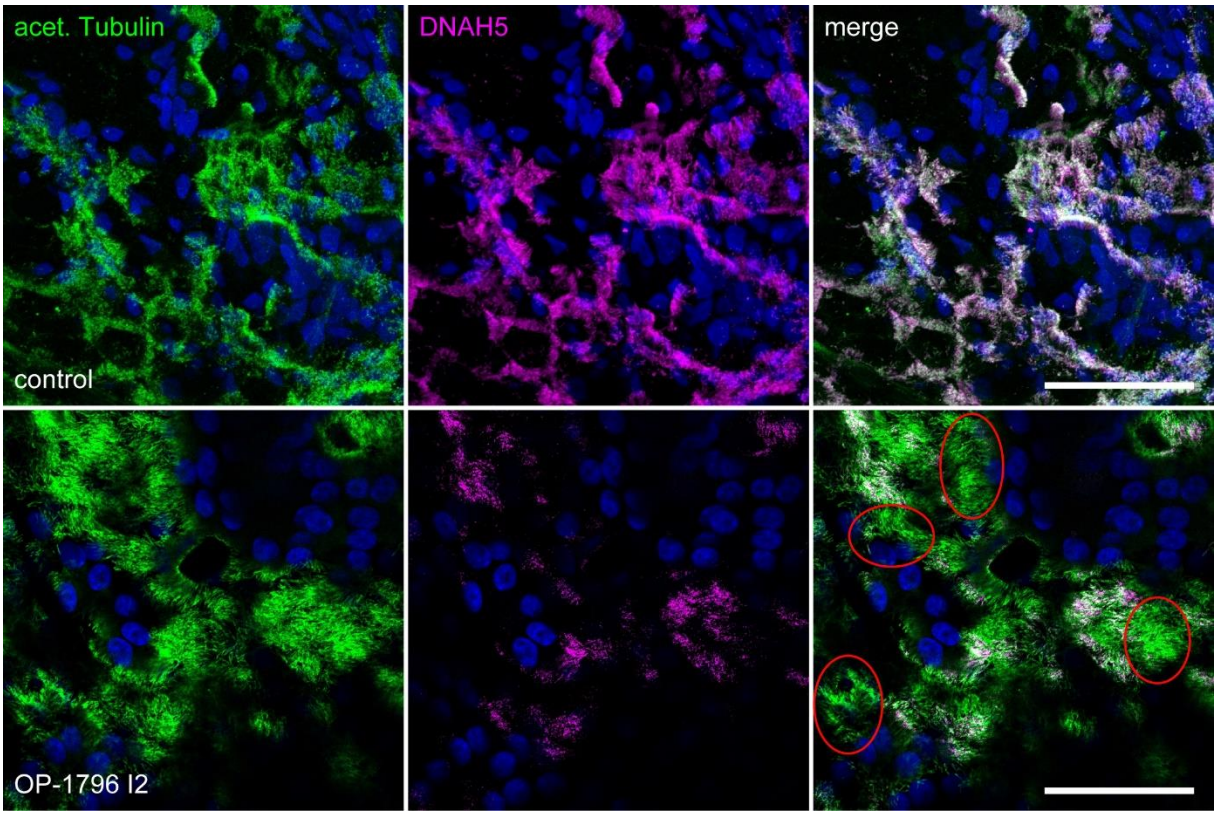

Supplementary Figure 13. Heterozygous DNAAF6 pathogenic variants in females result in a mosaic of cells with and without axonemal outer dynein arm defects. Respiratory epithelial cells from a female control individual and a female carrier (OP-1796 I2) with a heterozygous pathogenic *DNAAF6* variant were cultured under ALI conditions and double-labeled with antibodies directed against the outer dynein arm protein DNAH5 (magenta) and acetylated tubulin (green). Both proteins colocalize (white) along the ciliary axonemes in all cells from the unaffected control (upper panel). In OP-1796 I2, DNAH5 showed a normal axonemal localization in some cells or was completely absent or severely reduced (red circles) in the ciliary axonemes of other cells (lower panel). Nuclei were stained with Hoechst33342 (blue). Scale bars represent 50µm.

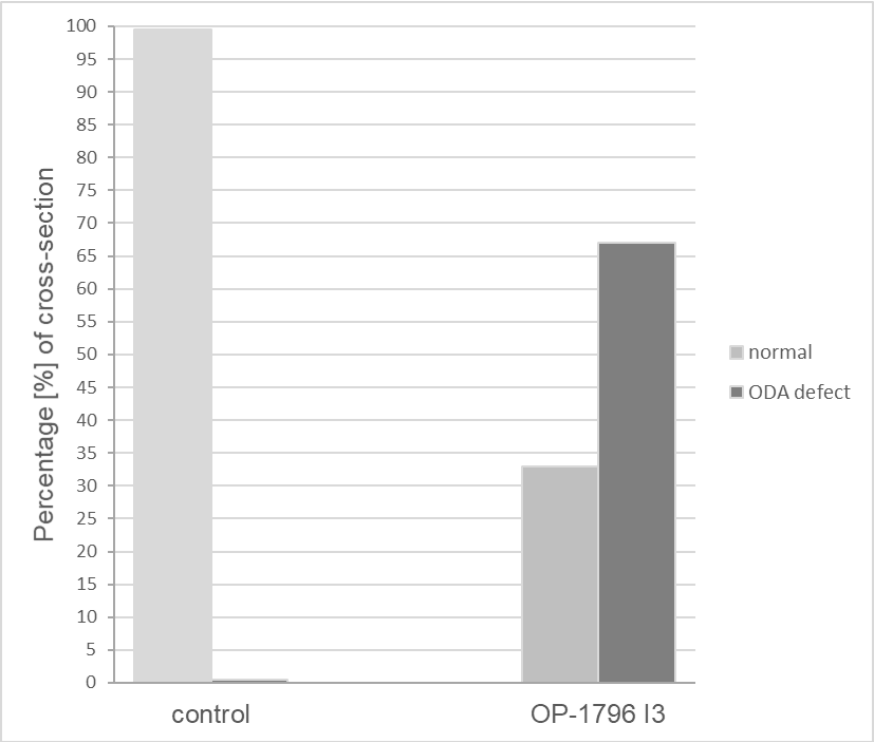

Supplementary Figure 14. Graphical summary of transmission-electron microscopy analysis of ciliary cross-sections from female individual OP-1796 I3 carrying a heterozygous variant in *DNAAF6* (n=1) and healthy controls (n=3). ODA was absent in more than half of the ciliated cells of OP-1796 I3 (67%; n=391 of 581 sections). In contrast, in control individuals, 99% of ciliary cross-sections showed normal ODA localization (n=429 of 431 sections).

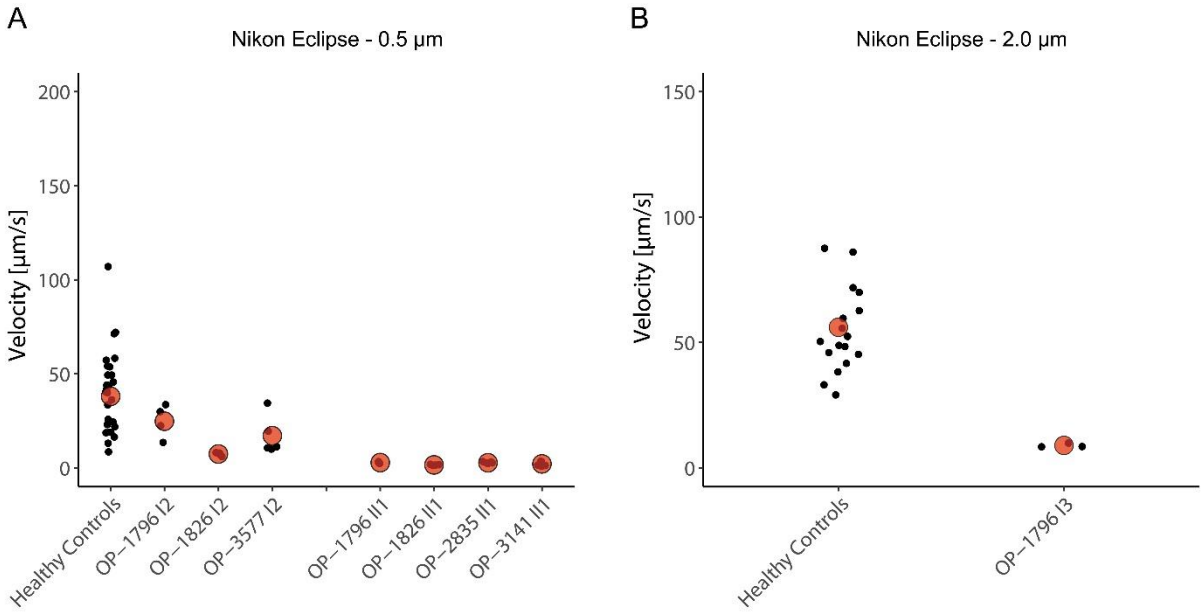

Supplementary Figure 15: *In vitro* ciliary transport assays in females with heterozygous pathogenic *DNAAF6* variants and males with hemizygous pathogenic *DNAAF6* variants.
A) Analyses performed on a Nikon Eclipse Ti-S phase-contrast microscope with ALI-inserts placed on a heating plate set to 37°C using 0.5µm fluorescent beads. Respiratory cells from a control group (mean velocity=38µm/s) and females with heterozygous *DNAAF6* variants (OP-1796 I2 (mean velocity=25µm/s); OP-1826 I2 (mean velocity=7.4µm/s); and OP-3577 I2 (mean velocity=17.2µm/s)) transported fluorescent particles in a linear direction along the cell layer. In contrast, the particle transport was non-oriented and significantly reduced in speed in male PCD individuals carrying hemizygous pathogenic variants in *DNAAF6* (OP-1796 II1 (mean velocity=3µm/s); OP-1826 II1 (mean velocity=1.6µm/s); OP-2835 II1 (mean velocity=2.7µm/s) and OP-3141 II1 (mean velocity=2.1µm/s)). The significantly reduced particle transport measured in the male PCD individuals (red dashed line) is a thermal driven background flow (Brownian movement). Red dots represent mean velocity.
B) Analyses performed on a Nikon Eclipse Ti-S phase-contrast microscope with ALI-inserts placed on a heating plate set to 37°C using 2µm fluorescent beads. Respiratory cells from a control group (mean velocity=56.1µm/s) and the female OP-1796 I3 carrying heterozygous *DNAAF6* variants (mean velocity=9µm/s) transported fluorescent particles in a linear direction along the cell layer. Red dots represent mean velocity.

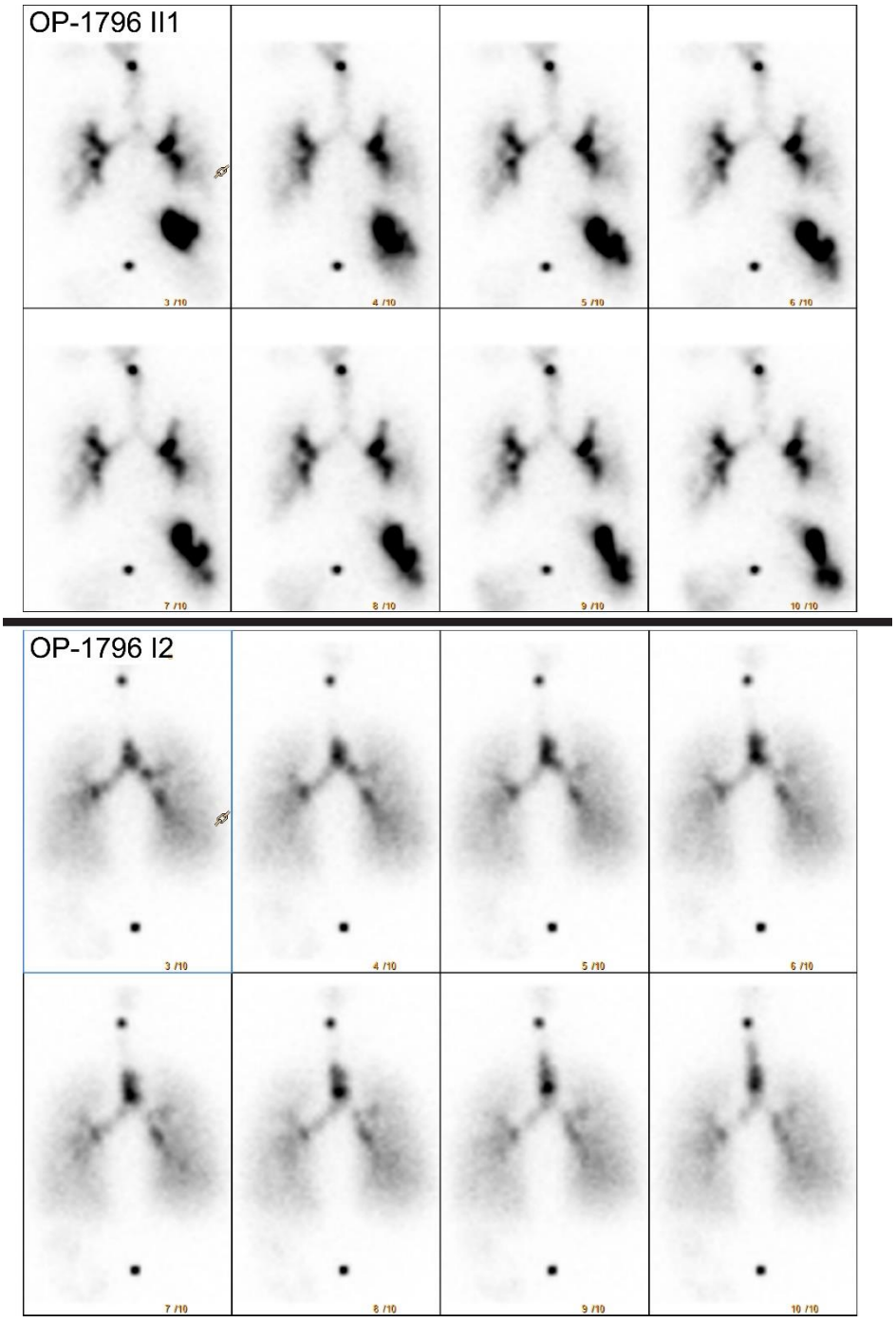

Supplementary Figure 16. *In vivo* assessment of pulmonary ciliary clearance capacity. Bronchioscintigraphy shows no bolus transport in the trachea of OP-1796 II1 carrying a hemizygous deletion in *DNAAF6*. Radioactivity is present in the stomach below the right lung (situs inversus). In contrast, the female individual OP-1796 I2 with a heterozygous deletion in *DNAAF6* presents with normal bolus transport within the trachea. Markers were placed over the neck and lumbar spine of both individuals.

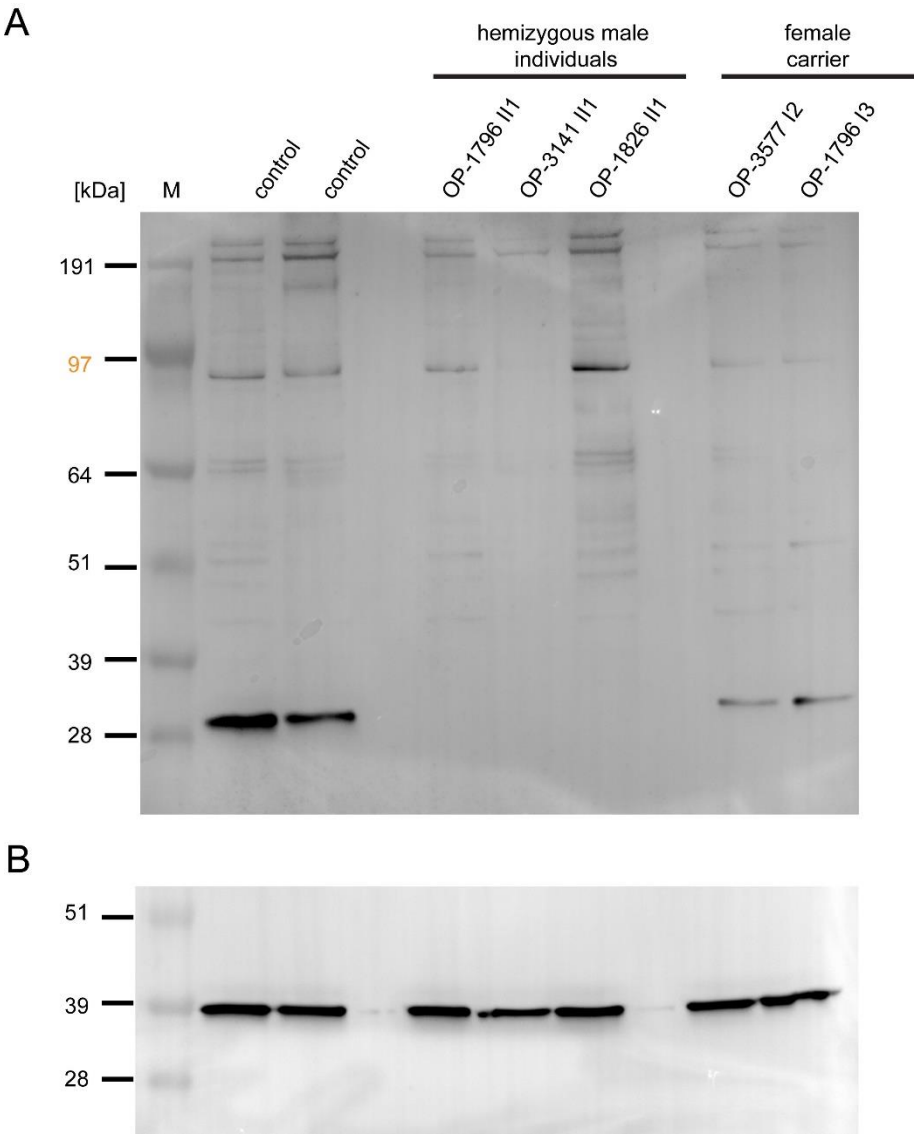

Supplementary Figure 17. DNAAF6 is absent in PCD individuals carrying hemizygous pathogenic variants in *DNAAF6*. (A) Immunoblot analysis using polyclonal antibodies directed against DNAAF6 (~25kDa) and respiratory cell lysates from healthy controls (females, n=2), male PCD individuals OP-1796 II1, OP-3141 II1, OP-1826 II1 and female carriers OP-3577 I2 and OP-1796 I3 showed absence of DNAAF6 in male PCD individuals and a marked reduction of DNAAF6 in female carriers. (B) Equal loading of protein content was verified using polyclonal antibodies directed against GAPDH (~36kDa). M=Protein standard; kDa: kiloDalton

Supplementary Movies

Supplementary Movie 1. Analysis of ciliary beating pattern of respiratory cilia from OP-1796 II1 by high-speed videomicroscopy.

Supplementary Movie 2. Analysis of ciliary beating pattern of respiratory cilia from OP-3141 II1 by high-speed videomicroscopy.

Supplementary Movie 3. Analysis of ciliary beating pattern of respiratory cilia from OP-1796 I2 by high-speed videomicroscopy.

Supplementary Movie 4. Analysis of ciliary beating pattern of respiratory cilia from OP-1796 I3 by high-speed videomicroscopy.

Supplementary Movie 5. Analysis of ciliary beating pattern of respiratory cilia from OP-1826 I2 by high-speed videomicroscopy.

Supplementary Movie 6. Analysis of ciliary beating pattern of respiratory cilia from OP-2835 II2 by high-speed videomicroscopy.

Supplementary Movie 7. Analysis of ciliary beating pattern of respiratory cilia from OP-3577 I2 by high-speed videomicroscopy.

Supplementary Movie 8. Analysis of ciliary beating pattern of control respiratory cilia by high-speed videomicroscopy.

Supplementary Movie 9. Pulmonary radioaerosol mucociliary clearance measurements for *in vivo* radiolabeled tracer in OP-1796 I2.

Supplementary Movie 10. Pulmonary radioaerosol mucociliary clearance measurements for *in vivo* radiolabeled tracer in OP-1796 II1.

Supplementary References

1. Tarkar A, Loges NT, Slagle CE, et al. (2013): DYX1C1 is required for axonemal dynein assembly and ciliary motility. Nat Genet 2013; 45:995–1003.
2. Richards S, Aziz N, Bale S, et al. Standards and guidelines for the interpretation of sequence variants: a joint consensus recommendation of the American College of Medical Genetics and Genomics and the Association for Molecular Pathology. Genetics in medicine: official journal of the American College of Medical Genetics 2015; 17:405-424.
3. Wang K, Li M, and Hakonarson H. ANNOVAR: functional annotation of genetic variants from high-throughput sequencing data. Nucleic acids research 2010; 38:e164.
4. Loges NT, Antony D, Maver A, et al. Recessive DNAH9 Loss-of-Function Mutations Cause Laterality Defects and Subtle Respiratory Ciliary-Beating Defects. *Am J Hum Genet* 2018;103:995-1008.
5. Fassad MR, Shoemark A, Legendre M, et al. Mutations in Outer Dynein Arm Heavy Chain DNAH9 Cause Motile Cilia Defects and Situs Inversus. Am J Hum Genet 2018, 103(6):984-994.
6. Olbrich H, Häffner K, Kispert A, et al. Mutations in DNAH5 cause primary ciliary dyskinesia and randomization of left-right asymmetry. Nat Genet 2002; 30(2):143-144.
7. Bartoloni L, Blouin JL, Pan Y, et al. Mutations in the DNAH11 (axonemal heavy chain dynein type 11) gene cause one form of situs inversus totalis and most likely primary ciliary dyskinesia. Proc Natl Acad Sci U S A. 2002 Aug 6;99(16):10282-6.
8. Schwabe GC, Hoffmann K, Loges NT, et al. Primary ciliary dyskinesia associated with normal axoneme ultrastructure is caused by DNAH11 mutations. Hum Mutat 2008; 29(2):289-298.
9. Pennarun G, Escudier E, Chapelin C, et al. Loss-of-function mutations in a human gene related to Chlamydomonas reinhardtii dynein IC78 result in primary ciliary dyskinesia. Am J Hum Genet 1999; 65(6):1508-15019.
10. Zariwala MA, Leigh MW, Ceppa F, et al. Mutations of DNAI1 in primary ciliary dyskinesia: evidence of founder effect in a common mutation. Am J Respir Crit Care Med 2006; 174(8):858-866.
11. Loges NT, Olbrich H, Fenske L, et al. DNAI2 mutations cause primary ciliary dyskinesia with defects in the outer dynein arm. Am J Hum Genet 2008;83:547-58.
12. Duriez B, Duquesnoy P, Escudier E, et al. A common variant in combination with a nonsense mutation in a member of the thioredoxin family causes primary ciliary dyskinesia. Proc Natl Acad Sci U S A 2007;104(9):3336-3341.
13. Mazor M, Alkrinawi S, Chalifa-Caspi V, Manor E, et al. Primary ciliary dyskinesia caused by homozygous mutation in DNAL1, encoding dynein light chain 1. Am J Hum Genet 2011;88(5):599-607.
14. Panizzi JR, Becker-Heck A, Castleman VH, et al. CCDC103 mutations cause primary ciliary dyskinesia by disrupting assembly of ciliary dynein arms. Nat Genet 2012;44(6):714-719.
15. Onoufriadis A, Paff T, Antony D, et al. Splice-site mutations in the axonemal outer dynein arm docking complex gene CCDC114 cause primary ciliary dyskinesia. Am J Hum Genet 2013;92(1):88-98.
16. Knowles MR, Leigh MW, Ostrowski LE, et al. Exome sequencing identifies mutations in CCDC114 as a cause of primary ciliary dyskinesia. Am J Hum Genet 2013;92(1):99-106.
17. Hjeij R, Lindstrand A, Francis R, et al. ARMC4 mutations cause primary ciliary dyskinesia with randomization of left/right body asymmetry. Am J Hum Genet 2013;93(2):357-367.

18. Hjeij R, Onoufriadis A, Watson CM, et al. CCDC151 mutations cause primary ciliary dyskinesia by disruption of the outer dynein arm docking complex formation. Am J Hum Genet 2014;95(3):257-274.

19. Wallmeier J, Shiratori H, Dougherty GW, et al. TTC25 Deficiency Results in Defects of the Outer Dynein Arm Docking Machinery and Primary Ciliary Dyskinesia with Left-Right Body Asymmetry Randomization. Am J Hum Genet 2016;99(2):460-469.

20. Bonnefoy S, Watson CM, Kernohan KD, et al. Biallelic Mutations in LRRC56, Encoding a Protein Associated with Intraflagellar Transport, Cause Mucociliary Clearance and Laterality Defects. Am J Hum Genet 2018; 103(5):727-739.

21. Loges NT, Olbrich H, Becker-Heck A, et al. Deletions and point mutations of LRRC50 cause primary ciliary dyskinesia due to dynein arm defects. Am J Hum Genet 2009; 85(6):883-889.

22. Duquesnoy P, Escudier E, Vincensini L, et al. Loss-of-function mutations in the human ortholog of Chlamydomonas reinhardtii ODA7 disrupt dynein arm assembly and cause primary ciliary dyskinesia. Am J Hum Genet 2009; 85(6):890-896.

23. Omran H, Kobayashi D, Olbrich H, et al. Ktu/PF13 is required for cytoplasmic pre-assembly of axonemal dyneins. Nature 2008;456(7222):611-616.

24. Mitchison HM, Schmidts M, Loges NT, et al. Mutations in axonemal dynein assembly factor DNAAF3 cause primary ciliary dyskinesia. Nat Genet 2012;44(4):381-389, S1-2.

25. Knowles MR, Ostrowski LE, Loges NT, et al. Mutations in SPAG1 cause primary ciliary dyskinesia associated with defective outer and inner dynein arms. Am J Hum Genet 2013 Oct 3;93(4):711-20.

26. Moore DJ, Onoufriadis A, Shoemark A, et al. Mutations in ZMYND10, a gene essential for proper axonemal assembly of inner and outer dynein arms in humans and flies, cause primary ciliary dyskinesia. Am J Hum Genet 2013; 93(2):346-56.

27. Zariwala MA, Gee HY, Kurkowiak M, et al. ZMYND10 is mutated in primary ciliary dyskinesia and interacts with LRRC6. Am J Hum Genet 20138;93(2):336-345.

28. Horani A, Druley TE, Zariwala MA, et al. Whole-exome capture and sequencing identifies HEATR2 mutation as a cause of primary ciliary dyskinesia. Am J Hum Genet 2012; 91(4):685-93.

29. Austin-Tse C, Halbritter J, Zariwala MA, et al. Zebrafish Ciliopathy Screen Plus Human Mutational Analysis Identifies C21orf59 and CCDC65 Defects as Causing Primary Ciliary Dyskinesia. Am J Hum Genet 2013;93(4):672-686.

30. Kott E, Duquesnoy P, Copin B, et al. Loss-of-function mutations in LRRC6, a gene essential for proper axonemal assembly of inner and outer dynein arms, cause primary ciliary dyskinesia. Am J Hum Genet 2012;91(5):958-964.

31. Horani A, Ferkol TW, Shoseyov D, et al. LRRC6 mutation causes primary ciliary dyskinesia with dynein arm defects. PLoS One 2013; 8(3):e59436.

32. Paff T, Loges NT, Aprea I et al. Mutations in PIH1D3 Cause X-Linked Primary Ciliary Dyskinesia with Outer and Inner Dynein Arm Defects. Am J Hum Genet 2017; 100:160–168.

33. Olcese C, Patel MP, Shoemark A, et al. X-linked primary ciliary dyskinesia due to mutations in the cytoplasmic axonemal dynein assembly factor PIH1D3. Nat Commun 2017; 8:14279.

34. Höben IM, Hjeij R, Olbrich H, et al. Mutations in C11orf70 Cause Primary Ciliary Dyskinesia with Randomization of Left/Right Body Asymmetry Due to Defects of Outer and Inner Dynein Arms. Am J Hum Genet 2018;102(5):973-984.

35. Fassad MR, Shoemark A, le Borgne P, et al. C11orf70 Mutations Disrupting the Intraflagellar Transport-Dependent Assembly of Multiple Axonemal Dyneins Cause Primary Ciliary Dyskinesia. Am J Hum Genet 2018; 102(5):956-972.

36. Moore A, Escudier E, Roger G, et al. RPGR is mutated in patients with a complex X linked phenotype combining primary ciliary dyskinesia and retinitis pigmentosa. J Med Genet 2006; 43(4):326-333.

37. Budny B, Chen W, Omran H, et al. A novel X-linked recessive mental retardation syndrome comprising macrocephaly and ciliary dysfunction is allelic to oral-facial-digital type I syndrome. Hum Genet 2006; 120(2):171-178.

38. Bustamante-Marin XM, Horani A, Stoyanova M, et al. Mutation of CFAP57, a protein required for the asymmetric targeting of a subset of inner dynein arms in Chlamydomonas, causes primary ciliary dyskinesia. PLoS Genet 2020; 16(8):e1008691.

39. Olbrich H, Schmidts M, Werner C, et al. Recessive HYDIN mutations cause primary ciliary dyskinesia without randomization of left-right body asymmetry. Am J Hum Genet 2012;91:672-84.

40. Cindrić S, Dougherty GW, Olbrich H, et al. SPEF2- and HYDIN-Mutant Cilia Lack the Central Pair-associated Protein SPEF2, Aiding Primary Ciliary Dyskinesia Diagnostics. Am J Respir Cell Mol Biol 2020;62(3):382-396.

41. Edelbusch C, Cindrić S, Dougherty GW, et al. Mutation of serine/threonine protein kinase 36 (STK36) causes primary ciliary dyskinesia with a central pair defect. Hum Mutat 2017;38(8):964-969.

42. Biebach L, Cindrić S, Koenig J, et al. Recessive Mutations in CFAP74 Cause Primary Ciliary Dyskinesia with Normal Ciliary Ultrastructure. Am J Respir Cell Mol Biol 2022;67(3):409-413.

43. Bustamante-Marin XM, Shapiro A, Sears PR, et al. Identification of genetic variants in CFAP221 as a cause of primary ciliary dyskinesia. J Hum Genet. 2020;65(2):175-180.

44. Kott E, Legendre M, Copin B, et al. Loss-of-function mutations in RSPH1 cause primary ciliary dyskinesia with central-complex and radial-spoke defects. Am J Hum Genet 2013; 93(3):561-570.

45. Knowles MR, Ostrowski LE, Leigh MW, et al. Mutations in RSPH1 cause primary ciliary dyskinesia with a unique clinical and ciliary phenotype. Am J Respir Crit Care Med 2014; 189(6):707-717.

46. Castleman VH, Romio L, Chodhari R, et al. Mutations in radial spoke head protein genes RSPH9 and RSPH4A cause primary ciliary dyskinesia with central-microtubular-pair abnormalities. Am J Hum Genet 2009; 84(2):197-209.

47. Jeanson L, Copin B, Papon JF, et al. RSPH3 Mutations Cause Primary Ciliary Dyskinesia with Central-Complex Defects and a Near Absence of Radial Spokes. Am J Hum Genet 2015; 97(1):153-162.

48. El Khouri E, Thomas L, Jeanson L, et al. Mutations in DNAJB13, Encoding an HSP40 Family Member, Cause Primary Ciliary Dyskinesia and Male Infertility. Am J Hum Genet 2016; 99(2):489-500.

49. Wirschell M, Olbrich H, Werner C, et al. The nexin-dynein regulatory complex subunit DRC1 is essential for motile cilia function in algae and humans. Nat Genet. 2013; 45(3):262-268.

50. Horani A, Brody SL, Ferkol TW, et al. CCDC65 mutation causes primary ciliary dyskinesia with normal ultrastructure and hyperkinetic cilia. PLoS One 2013; 8(8):e72299.

51. Olbrich H, Cremers C, Loges NT, et al. Loss-of-Function GAS8 Mutations Cause Primary Ciliary Dyskinesia and Disrupt the Nexin-Dynein Regulatory Complex. Am J Hum Genet 2015;97(4):546-554.

52. Merveille AC, Davis EE, Becker-Heck A, et al. CCDC39 is required for assembly of inner dynein arms and the dynein regulatory complex and for normal ciliary motility in humans and dogs. Nat Genet 2011;43(1):72-78.

53. Becker-Heck A, Zohn IE, Okabe N, et al. The coiled-coil domain containing protein CCDC40 is essential for motile cilia function and left-right axis formation. Nat Genet. 2011; 43(1):79-84.

54. Wallmeier J, Al-Mutairi DA, Chen CT, et al. Mutations in CCNO result in congenital mucociliary clearance disorder with reduced generation of multiple motile cilia. Nat Genet 2014; 46(6):646-651.

55. Boon M, Wallmeier J, Ma L, et al. MCIDAS mutations result in a mucociliary clearance disorder with reduced generation of multiple motile cilia. Nat Commun 2014; 5:4418.

56. Wallmeier J, Frank D, Shoemark A, et al. De Novo Mutations in FOXJ1 Result in a Motile Ciliopathy with Hydrocephalus and Randomization of Left/Right Body Asymmetry. Am J Hum Genet 2019 Nov 7; 105(5):1030-1039.

57. Wallmeier J, Bracht D, Alsaif HS, et al. Mutations in TP73 cause impaired mucociliary clearance and lissencephaly. Am J Hum Genet 2021; 108(7):1318-1329.

58. Narasimhan V, Hjeij R, Vij S, et al. Mutations in CCDC11, which encodes a coiled-coil containing ciliary protein, causes situs inversus due to dysmotility of monocilia in the left-right organizer. Hum Mutat 2015; 36(3): 307-318.

59. Sigg MA, Menchen T, Lee C, et al. Evolutionary Proteomics Uncovers Ancient Associations of Cilia with Signaling Pathways. Dev Cell 2017; 43(6):744-762.e11.

60. Bustamante-Marin XM, Yin WN, Sears PR, et al. Lack of GAS2L2 Causes PCD by Impairing Cilia Orientation and Mucociliary Clearance. Am J Hum Genet 2019; 104(2): 229-245.

61. Chivukula RR, Montoro DT, Leung HM, et al. A human ciliopathy reveals essential functions for NEK10 in airway mucociliary clearance. Nat Med 2020; 26(2): 244-251.

62. Thomas L, Bouhouche K, Whitfield M, et al. TTC12 Loss-of-Function Mutations Cause Primary Ciliary Dyskinesia and Unveil Distinct Dynein Assembly Mechanisms in Motile Cilia Versus Flagella. Am J Hum Genet 2020; 106(2):153-169.

63. Beydon N, Kouis P, Marthin JK et al. Nasal nitric oxide measurement in children for the diagnosis of primary ciliary dyskinesia: European Respiratory Society technical standard. Eur Respir J 2023; 61(4):2202031.

64. Sisson JH, Stoner JA, Ammons B et al. All-digital image capture and whole-field analysis of ciliary beat frequency. J Microsc 2003; 211:103–111.

65. Raidt J, Wallmeier J, Hjeij R et al. Ciliary beat pattern and frequency in genetic variants of primary ciliary dyskinesia. Eur Respir J 2014; 44:1579-1588.

66. Munkholm M, Nielsen KG, Mortensen J. Clinical value of measurement of pulmonary radioaerosol mucociliary clearance in the work up of primary ciliary dyskinesia. EJNMMI Res 2015; 5:118.

67. Marthin JK, Mortensen J, Pressler T et al. Pulmonary radioaerosol mucociliary clearance in diagnosis of primary ciliary dyskinesia. Chest 2007; 132:966-976.

68. Mortensen J, Lange P, Nyboe J et al. Lung mucociliary clearance. Eur J Nucl Med 1994; 21:953-961.

69. Marthin JK, Holgersen MG, Nielsen KG et al. Pulmonary radioaerosol mucociliary clearance assessment: searching for genotype-specific differences and potential as an outcome measure in primary ciliary dyskinesia. ERJ Open Res. 2023; 9(6):00685-2023.

70. Marthin JK, Nielsen KG, Mortensen J. Quantitative 99mTc-albumin colloid Nasal Mucociliary Clearance as outcome in primary ciliary dyskinesia. ERJ Open Res 2023; 9(5):00345-2023.

71. Omran H, Loges NT. Immunofluorescence staining of ciliated respiratory epithelial cells. Methods Cell Biol 2009; 91:123-133.

72. Dougherty GW, Loges NT, Klinkenbusch JA et al. DNAH11 Localization in the Proximal Region of Respiratory Cilia Defines Distinct Outer Dynein Arm Complexes. Am J Respir Cell Mol Biol 2016; 55:213-224.

73. Olbrich H, Schmidts M, Werner C et al. Recessive HYDIN mutations cause primary ciliary dyskinesia without randomization of left-right body asymmetry. Am J Hum Genet 2012; 91:672-684.